








ORIGINAL RESEARCH

# miR-133a Replacement Attenuates Thoracic Aortic Aneurysm in Mice

Adam W. Akerman , PhD; Elizabeth N. Collins, BS; Andrew R. Peterson, BS; Lauren B. Collins , BS; Jessica K. Harrison , BS; Amari DeV Vaughn , BS; Jaleel M. Townsend, BS; Rebecca L. Vanbuskirk , BS; Jessica Riopedre-Maqueira, BS; Ailet Reyes, BS; Joyce E. Oh , BS; Charles M. Raybuck, BS; Jeffrey A. Jones, PhD; John S. Ikonomidis , MD, PhD

**BACKGROUND:** Thoracic aortic aneurysms (TAAs) occur because of abnormal remodeling of aortic extracellular matrix and are accompanied by the emergence of proteolytically active myofibroblasts. The microRNA miR-133a regulates cellular phenotypes and is reduced in clinical TAA specimens. This study tested the hypothesis that miR-133a modulates aortic fibroblast phenotype, and overexpression by lentivirus attenuates the development of TAA in a murine model.

**METHODS AND RESULTS:** TAA was induced in mice. Copy number of miR-133a was reduced in TAA tissue and linear regression analysis confirmed an inverse correlation between aortic diameter and miR-133a. Analyses of phenotypic markers revealed an mRNA expression profile consistent with myofibroblasts in TAA tissue. Fibroblasts were isolated from the thoracic aortae of mice with/without TAA. When compared with controls, miR-133a was reduced, migration was increased, adhesion was reduced, and the ability to contract a collagen disk was increased. Overexpression/knockdown of miR-133a controlled these phenotypes. After TAA induction in mice, a single tail-vein injection of either miR-133a overexpression or scrambled sequence (control) lentivirus was performed. Overexpression of miR-133a attenuated TAA development. The pro-protein convertase furin was confirmed to be a target of miR-133a by luciferase reporter assay. Furin was elevated in this murine model of TAA and repressed by miR-133a replacement in vivo resulting in reduced proteolytic activation.

**CONCLUSIONS:** miR-133a regulates aortic fibroblast phenotype and over-expression prevented the development of TAA in a murine model. These findings suggest that stable alterations in aortic fibroblasts are associated with development of TAA and regulation by miR-133a may lead to a novel therapeutic strategy.

**Key Words:** fibroblast ■ furin ■ miR-133a ■ myofibroblast ■ thoracic aortic aneurysm

**T**horacic aortic aneurysm (TAA) disease commonly results in increased morbidity and mortality. Treatment options are limited and continue to be a difficult management problem for cardiovascular surgeons. A TAA is a localized, progressive dilatation of the supradiaphragmatic aorta with a cross-sectional diameter >50% its normal size. Aneurysms develop as a consequence of atypical extracellular matrix (ECM) remodeling.<sup>1</sup> Endogenous vascular cells, such as fibroblasts, function to balance ECM deposition and degradation to maintain aortic wall integrity. In TAA, this

balance is disrupted, allowing for enhanced proteolysis, which leads to progressive dilation. Breakdown of typically durable ECM molecules, such as elastin and collagen, involves the matrix metalloproteinases (MMPs).<sup>2,3</sup> These proteolytic enzymes can process all matrix components. Some MMPs are secreted while others are membrane bound. The membrane-type MMPs play a dual role in aneurysm progression by contributing to pericellular proteolysis and activation of intracellular signaling pathways.<sup>4</sup> Proteolytic activation and subsequent cell surface presentation of the

Correspondence to: John S. Ikonomidis, MD, PhD, Division of Cardiothoracic Surgery, University of North Carolina, Chapel Hill, NC 27514. E-mail: john\_ikonomidis@med.unc.edu

Supplementary Materials for this article are available at <https://www.ahajournals.org/doi/suppl/10.1161/JAHA.120.019862>

For Sources of Funding and Disclosures, see page 17.

© 2021 The Authors. Published on behalf of the American Heart Association, Inc., by Wiley. This is an open access article under the terms of the Creative Commons Attribution-NonCommercial-NoDerivs License, which permits use and distribution in any medium, provided the original work is properly cited, the use is non-commercial and no modifications or adaptations are made.

JAHA is available at: [www.ahajournals.org/journal/jaha](http://www.ahajournals.org/journal/jaha)

## CLINICAL PERSPECTIVE

### What Is New?

- MicroRNA miR-133a regulates aortic fibroblast phenotype and systemic overexpression prevented aneurysm formation in a mouse model of thoracic aortic aneurysm.

### What Are the Clinical Implications?

- Regulation of aortic tissue miR-133a levels may lead to a novel therapeutic strategy for thoracic aortic aneurysm disease.

## Nonstandard Abbreviations and Acronyms

<b>ddPCR</b>	droplet digital polymerase chain reaction
<b>DDR2</b>	discoidin domain receptor family, member 2
<b>ECM</b>	extracellular matrix
<b>MMPs</b>	matrix metalloproteinases
<b>MT1-MMP</b>	membrane type 1 matrix metalloproteinase
<b>Myh11</b>	smooth muscle myosin
<b>TAA</b>	thoracic aortic aneurysm
<b>UTR</b>	untranslated region

prototypical membrane type 1 MMP (MT1-MMP) requires processing by the pro-protein convertase furin. This pathway has been attributed to ECM remodeling and cellular phenotype transformation. However, regulation of this pathway has yet to be applied for therapeutic advantage.

Dilation of the thoracic aorta is accompanied with apoptosis of smooth muscle cells.<sup>2,5,6</sup> Accordingly, as the aneurysm progresses and the smooth muscle cell content within the aortic wall declines, resident fibroblasts become the principal cell type remaining and likely function to manage the vascular remodeling process. In addition to alterations in cell number, it has been proposed that the endogenous fibroblasts may undergo a transformation in phenotype, exhibiting properties of myofibroblasts.<sup>7</sup> Myofibroblasts are known to contribute to vascular remodeling.<sup>8</sup> It has been suggested that this phenotypic transformation may be regulated by a class of small noncoding RNA molecules, known as the microRNAs.<sup>9</sup> Repression of translation occurs when a portion of the microRNAs sequence, known as the seed region, interacts most commonly with the 3'-untranslated region of a given mRNA transcript. Interestingly, binding of the

seed region may occur with multiple different mRNA transcripts, suggesting one microRNA may have the unique ability to regulate a coordinated cassette of genes to influence cellular phenotype.<sup>10,11</sup>

Using clinical TAA specimens, this laboratory has established that the mature levels, or portion that is taken up by the RNA-induced silencing complex,<sup>12</sup> of several microRNAs display an inverse linear correlation with aortic diameter.<sup>13</sup> Some, including miR-133a, were proportionally reduced as diameter increased.<sup>14</sup> The significance of miR-133a in regulation of cellular phenotype, and subsequent ECM remodeling in cardiovascular tissues is beginning to be understood. This suggests that the loss of miR-133a may contribute to pathological changes in the thoracic aorta during aneurysm development. Thus, the aim of the current study was to determine the effects of miR-133a on TAA development in a murine model that recapitulates the hallmarks of clinical pathology. Accordingly, this investigation tested the hypothesis that miR-133a regulates aortic fibroblast phenotype and the development of TAA.

## METHODS

The data, analytic methods, and study materials will be made available to other researchers for purposes of reproducing the results or replicating the procedures upon request.

### Animal Care

All procedures were performed in accordance with the National Research Council's *Guide for the Care and Use of Laboratory Animals* and approved by the institutional animal care and use committee of the University of North Carolina at Chapel Hill Institutional Animal Care and Use Committee (Protocol: 17-203). Wild-type C57BL/6 mice (Envigo, Hackensack, NJ) were bred in-house and used for this study beginning at 10 weeks of age.

### TAA Induction in Mice

Surgical induction of TAA in mice was performed by methods previously described.<sup>15</sup> In short, mice anesthetized with isoflurane were intubated and mechanically ventilated. A left posterolateral thoracotomy was performed at the sixth intercostal space. Images of the exposed descending thoracic aorta were captured on a calibrated video microscopy system (PAXcam using PAX-it image analysis software, version 1.4.1; MIS Inc, Lakeland, FL) and were used to measure aortic diameter. Aneurysms were induced by applying a sponge soaked in CaCl<sub>2</sub> (0.5 mol/L) to the distal descending thoracic aorta for 15 minutes followed by chest closure. After 4, 8, or 16 weeks,

the descending thoracic aorta was measured for comparison, and the difference was expressed as percentage change in aortic diameter from baseline. An aneurysm was defined as a dilation of >50% baseline measurement. The descending thoracic aorta was harvested for biochemical or histological analysis. An even number of male and female mice were included when possible and were compared with age- and weight-matched litter-mate controls. Sample sizes for each experiment are listed in each respective figure legend.

### RNA Copy Number Quantification

Total RNA was extracted by ethanol precipitation using TRIzol Reagent (15596026, Thermo Fisher Scientific, Waltham, MA) and quantified by NanoDrop 2000 (Thermo Fisher Scientific). For cellular and tissue microRNA quantification, cDNA was synthesized from 150 ng of total RNA and before polymerase chain reaction amplification was diluted with RNase-free water (1:2). For mRNA and primary miRs, cDNA was synthesized from 1 µg of total RNA using the qScript cDNA synthesis kit (95047, Quantabio, Beverly, MA); before polymerase chain reaction amplification of mRNAs, cDNA was diluted in RNase-free water (1:2). For analysis of the primary microRNAs, cDNA was not diluted before droplet generation and polymerase chain reaction amplification. These dilutions allowed for a minimum count of 100 copies of each RNA copy to be measured in each droplet digital polymerase chain reaction (ddPCR) reaction. For each ddPCR assay, 5 µL cDNA sample, 12.5 µL ddPCR supermix for probes (no dUTP) (1863024; Bio-Rad Laboratories, Hercules, CA), and 5 µL RNase-free water was added to the mixture. For microRNAs, 1.25 µL miR-133a Fam labeled probe and 1.25 µL U6 VIC labeled probe were added to the mixture. Mature miR-133a levels were standardized to levels of the small nuclear RNA, U6 in a multiplexed reaction. For murine mRNAs and primary miRs, a 1× concentration of the following FAM labeled probes for primary miR-133a-1, primary miR-133a-2, vimentin, desmin, von Willebrand factor, discoidin domain receptor family, member 2 (DDR2), smooth muscle myosin (Myh11), or alpha smooth muscle actin were multiplexed with VIC labeled GAPDH probe. All primer and gene target information is available in Table. Information concerning specificity, linear dynamic range, sensitivity, and efficiency in gene expression analyses is available online at <https://www.thermofisher.com/order/genome-database/> and can be found for each TaqMan gene expression assay by searching the catalog numbers provided in Table. The mixture and 70 µL of droplet generation oil for probes (1863005; Bio-Rad Laboratories) were loaded into the sample

and oil wells of a disposable droplet generator cartridge (1864008; Bio-Rad Laboratories). Droplets were generated by the QX-200 droplet generator (Bio-Rad Laboratories) and carefully transferred to a 96-well polymerase chain reaction plate by pipetting the mixture down the side of the well at an angle. The plate was sealed with foil at 180°C. The thermo cycling conditions were 95°C for 10 minutes, 94°C for 30 seconds, 60°C for 1 minute, repeat 39 times from step 2, 98°C for 10 minutes, and 4°C for 30 minutes, after which the plate was incubated at room temperature for 5 minutes. Droplets were read in the QX200 droplet reader (Bio-Rad Laboratories). Only samples containing >10 000 droplets were included in analysis of copy number determination. Poisson distribution was used to determine the number of template molecules per droplet using Quantasoft Analysis Pro (Bio-Rad Laboratories). Normalization was performed by dividing all copy numbers by the internal referent controls GAPDH, for mRNAs and primary miRs, and U6 snRNA for miR-133a.

### Cell Culture

Primary aortic fibroblast cell lines (n=10) were established from murine biopsies of control and aneurysmal thoracic aortas using an established outgrowth technique as previously described.<sup>16</sup> Cell cultures were confirmed to be solely fibroblast by ddPCR. Fibroblast cultures were defined as having a positive mRNA signal for vimentin and DDR2, while negative for smooth muscle cell desmin and endothelial-specific von Willebrand factor. The isolated aortic fibroblasts were maintained in complete fibroblast-specific growth media (Fibroblast growth media 2; C-23020, PromoCell, Heidelberg, Germany) with added 10% fetal bovine serum (1600; Gibco), and gentamicin (0.5 mg/mL; 15710-064, Gibco) at 37°C in 5% CO<sub>2</sub>. Aortic fibroblasts from culture passages 2 to 10 were used in the following cellular phenotypic studies.

### Fibroblast Migration

A transwell assay was used to compare migration capacity of control and TAA fibroblasts. Thirty-two thousand aortic fibroblasts per well were seeded into the upper chamber of the 8.0-µm pore fluroblock membrane of the transwell chamber (351152; Corning) in serum-free (basal) fibroblast growth media. Complete fibroblast growth media with 10% fetal bovine serum was added to the lower chamber. The cells were maintained under normal tissue culture conditions for 24 hours, and the membranes were fixed by immersion in methanol at room temperature for 30 minutes. Nuclei were stained with DAPI. Membranes were imaged and counted by microscopy (10×) (Revolve; Echo,

**Table. PCR Primer and Gene Target Information**

Full Name	Abbreviation	Catalogue Number	Accession Number	Dye
hsa-miR-133a-1	miR-133a	002246	MI0000450	FAM
SNO-U6	U6	001973	NR_004394.1	VIC
primary-miR-133a-1	pri-miR-133a-1	Mm03306281_pri	MI0000159	FAM
primary-miR-133a-2	pri-miR-133a-2	Mm03307401_pri	MI0000820	FAM
Myosin Heavy Chain 11	Myh11	Mm00443013_m1	NM_001161775.1	FAM
Discoidin domain receptor 2	DDR2	Mm00445615_m1	NM_022563.2	FAM
Vimentin	Vimentin	Mm01333430_m1	NM_011701.4	FAM
Desmin	Desmin	Mm00802455_m1	NM_010043.2	FAM
Von Willebrand Factor	vWF	Mm00550376_m1	NM_011708.4	FAM
Alpha Smooth Muscle Actin	$\alpha$ -SMA	Mm01204962_gh	NM_007392.3	FAM
Glyceraldehyde 3-phosphate dehydrogenase	GAPDH	Mm9999915_g1	NM_001289726.1	VIC

A detailed list of all gene targets with full names and abbreviations used in this publication. Additionally, the Life Technologies Catalogue number and National Center for Biotechnology Information (NCBI) accession numbers are included. The dye column refers to the fluorescent label conjugated to hydrolysis probes used in multiplexed ddPCR reactions. FAM indicates 6-Carboxyfluorescein; and VIC, 2'-chloro-7'-phenyl-1,4-dichloro-6-carboxy-fluorescein.

San Diego, CA) in 5 separate areas on both sides of the membrane, and an average cell count for each side was calculated. The percentage migration was determined by dividing the average of the bottom membrane count by sum of cells on top and bottom.

### Fibroblast Adhesion

Six thousand control or TAA aortic fibroblasts were added to the wells of black wall, clear bottom 96-well plates (3631; Corning). Duplicate plates were prepared (washed and unwashed) for comparative analysis to account for minor variations in cell count. All plates were incubated at 37°C for exactly 1 hour to allow for adherence. One of the duplicate plates was washed with PBS 5 times using an automated plate washer (Aquamax 200 with cell wash head; Molecular Devices, Sunnyvale, CA), and both plates were then incubated with Cyquant (C7026; Thermo Fisher Scientific) for 1 hour. Nuclei of adhered fibroblasts were counted on the Spectramax i3x with the MiniMax300 imaging cytometer (Molecular Devices). Each cell line was an average count of 8 replicate wells. Washed plates were compared with unwashed plates, and the difference was represented as fold change from unwashed.

### Fibroblast Contraction

Contraction was measured in cultured fibroblasts using an established collagen disk assay.<sup>17</sup> In short, control and TAA fibroblasts were incorporated in disks of rat tail collagen type I (1 mg/mL in complete growth media) polymerized in a 24-well non-tissue culture-treated plate (3738; Costar); 50 000 fibroblasts were incorporated in each disk, and each cell line was assayed in triplicate. Images of the disk were taken (1x) at 1, 3, 5,

6, and 7 hours, and the disc area was measured with ImageJ. Area versus time was plotted in SigmaPlot 14 (Systat Software, San Jose, CA), and linear regression was used to express the rate of contraction (mm<sup>2</sup>/h).

### In Vitro Transfection

Transfection of aortic fibroblasts was performed in 75 cm<sup>2</sup> flask (430641U; Corning) with jetPRIME (114-15, Polypolus-transfection) 3 times, 24 hours apart, using 10  $\mu$ g MISSION microRNA mimic or inhibitor (anti-miR-133a). Cells were transfected with negative control (HMC0003; Sigma-Aldrich, St. Louis, MO), miR-133a (HMI0196; Sigma-Aldrich), or anti-miR-133a (HSTUD0196; Sigma-Aldrich). Transfected cells were then subjected to the above phenotypic assays.

### In Vivo Lentiviral Delivery

For in vivo miR-133a over expression, the pMIRNA1 lentiviral vector (PMIRmiR-133a-1PA-1; System Biosciences, Mountain View, CA) was used to overexpress the murine miR-133a-1 precursor under control of the cytomegalovirus promoter in aortic tissue by methods previously described.<sup>18</sup> Additionally, these vectors are bicistronic for the green fluorescent protein under control of the elongation factor 1 promoter. In short, either the miR-133a lentivirus, or control virus (CD511B-1; System Biosciences) was diluted to a concentration of 1x10<sup>9</sup> PFU/100  $\mu$ L in normal saline. Optimal titer of lentivirus was selected based on results from a pilot investigation (Figure S1). Intravenous injection was performed via tail vein with 100  $\mu$ L of virus solution followed by a 100  $\mu$ L saline chase using a 33-gauge low-dead-space needle (LDS-3009; TSK) 24 hours following the induction surgery. This lentiviral expression system has been demonstrated to infect almost any mammalian cell type, including nondividing

cells and whole-model organisms. Viral injection was well tolerated, with no observed adverse side effects or mortality.

### Perfusion Fixation, Histology, and Immunohistochemistry

Thoracic aortas from control and TAA mice were perfusion fixed in 10% formalin at  $\approx 100$  mm Hg and subsequently soaked in 10% formalin overnight. Aortic segments were transferred to 70% ethanol for storage at 4°C. Fixed aortic segments were embedded in paraffin and sectioned at 5  $\mu$ m thickness. In preparation for staining and immunohistochemistry, tissue sections were deparaffinized and rehydrated. Deparaffinized slides were stained with a modified elastic Verhoeff–Van Gieson stain (HT251; Sigma-Aldrich), dehydrated to absolute alcohol, cover slipped with resin-based slide mounting media, and examined by microscopy (40 $\times$ ) (Echo Revolve). For immunofluorescence, deparaffinized slides were washed in TBS+0.025% Triton X-100, blocked in 10% normal serum with 1% BSA in TBS for 2 hours at room temperature. Anti-turbo green fluorescent protein primary antibody (1:1000, AB513; Evrogen, Moscow, Russia) diluted in TBS was applied to the aortic tissue and incubated overnight at 4°C. Slides were rinsed in TBS 0.025% Triton-X and incubated in the dark with Alexa Fluor 594 (10  $\mu$ g/mL in TBS) (A32740; Thermo Fisher Scientific) for 1 hour at room temperature. Nuclei were stained with DAPI then imaged at 40 $\times$  with red, green, and blue epifluorescence channels.

### Luciferase Reporter Assay

HT1080 cells, at a confluence of 70%, were cotransfected with DharmaFECT-Duo transfection reagent and either the miR-133a mimic or a non-mRNA targeting control (100 nmol/L) and 3  $\mu$ g of one of the following vectors from Switchgear Genomics: the furin 3' untranslated region (UTR; S809837), which contains the furin 3'UTR cloned downstream of the luciferase gene; the mutated furin 3'UTR, which contains the site-directed mutagenesis replacing the putative miR-133a binding site, CUGGU for GACCA, in the furin 3'UTR cloned downstream of the luciferase gene; the random sequence 3'UTR, which contains nonconserved, nongenic, and nonrepetitive human genomic fragments cloned downstream from the luciferase gene; and the empty 3'UTR vector (S8090005), which contains only the luciferase gene and its constitutive promoter, to serve as the positive control. Reporter assays were performed 24 hours following transfection by the LightSwitch Luciferase Assay system (LS010; SwitchGear Genomics, Menlo Park, CA). Luminescence was quantitated by luminometer (Spectramax i3X; Molecular Devices). All

transfection experiments were performed 4 times in triplicate.

### Immunoblotting

For tissue samples, thoracic aortas were homogenized in Halt Protease Inhibitor Cocktail (87785; ThermoFisher Scientific) diluted in PBS. For cells, 1 million aortic fibroblasts were lifted with TrypLE (12604021; Thermo Fisher Scientific), pelleted, and resuspended in the Halt Protease Inhibitor Cocktail. For both tissue and cell samples, a portion of the sample was taken for total protein quantification using the Pierce bicinchoninic acid protein assay kit (23225; Thermo Fisher Scientific). A 1:1 dilution of the suspension to Laemmli buffer was heated at 90°C for 10 minutes and snap frozen at  $-80^{\circ}\text{C}$ . Equal amounts of total protein (10  $\mu$ g) were loaded onto 4% to 15% Mini-PROTEAN TGX Stain-Free Gels (4568084; Bio-Rad Laboratories) and transferred onto nitrocellulose membranes (88018, Thermo Fisher Scientific). After blocking for 1 hour in 5% BSA (97061-422; VWR) at room temperature, the membranes were incubated for 1 hour at room temperature in primary antisera for active MT1-MMP (AB8221, Chemicon; tissue: 1:5000, cells: 1:10 000) or furin (ab3467, Abcam; tissue: 1:1000, cells: 1:5000), and GAPDH (VPA00187, Bio-Rad Laboratories; tissue: 1:5000, cells: 1:5000). Membranes were washed in TBST, incubated for 1 hour at room temperature in horseradish peroxidase labeled Goat-Anti-Rabbit secondary antibody (GtxRb-003-EHRPC; Immunoreagent Inc, Raleigh, NC; tissue and cells: 1:5000), and washed in TBST. Chemiluminescent substrate activation was performed with SuperSignal West Pico PLUS following manufacturers protocols (34580; Thermo Fisher Scientific). The immunoreactive signals were analyzed using densitometric methods (ImageJ) to obtain 2-dimensional integrated optical density values. All samples were normalized to their respective GAPDH abundance.

### Statistical Analysis

Statistical analyses were performed using SigmaPlot, 14 (Systat). Sample size for experiments was based on a prior study comparing similar primary readouts between experimental groups (aortic tissue miR-133a levels).<sup>19</sup> In short, power calculations using an ANOVA model were completed assuming a 25.5% minimum detectable difference in means with a pooled SD (across 3 groups) of 7.4%. Therefore, to provide hypothesis testing at a desired power of 0.95 with an  $\alpha$  level of 0.05, sample size was determined to be a minimum of 5 per group. Thus, all experiments in this study included a sample size of  $>5$ . Relationships between miR-133a copy number and aortic diameter were determined using linear least-squares regression

analysis. Results were reported graphically, and a correlation constant ( $r$  value) and  $P$  value were determined (Systat Linear Regression). Two sample mean comparisons were made with both the Student  $t$  test and Welch's  $t$  test. In the event different  $P$  values were obtained, the higher of the 2 values is reported. All data were assessed for normality using the Shapiro-Wilk test, and the corresponding appropriate statistical test and sample sizes are listed in each respective figure legend with  $P$  values. Raw data are displayed next to the group mean, median, and standard error of the mean. Effect size calculations were performed using Cohen's  $d$  test unless there were differences in sample size. For comparisons with different sample sizes, effect size was determined using Hedges'  $g$  test. For each effect size value an effect level was assigned using the following scheme:  $<0.1$ : trivial; 0.1 to 0.3: small; 0.3 to 0.5: medium;  $>0.5$ : large. A summary is provided in Table S1. For all comparisons, a  $P$  value of  $<0.05$  was considered significant.

## RESULTS

### MiR-133a Was Decreased in TAA Tissue

TAA was induced in mice. Vessel dilation was measured during the terminal surgery and analyzed as a percentage change from baseline diameter. Following TAA induction, the diameter of the descending thoracic

aorta was increased at 4 weeks ( $59.50\pm 4.90\%$ ;  $n=9$ ;  $P<0.001$ ), 8 weeks ( $64.25\pm 6.77\%$ ;  $n=10$ ;  $P<0.001$ ), and 16 weeks ( $62.89\pm 6.75\%$ ;  $n=8$ ;  $P<0.001$ ) after aneurysm induction when compared with baseline measurements. Formation of aneurysm (a  $>50\%$  dilation) occurred by 4 weeks and no differences in diameter were detected between 4-, 8-, and 16-week cohorts ( $P=0.854$ ) (Figure 1A). Quantification of mature miR-133a copy number in aortic tissues identified miR-133a was decreased at 4 weeks ( $0.45\pm 0.082$  copies per U6;  $n=7$ ;  $P=0.623$ ), and significantly reduced at 8 weeks ( $0.19\pm 0.073$  copies per U6;  $n=7$ ;  $P=0.004$ ), and 16 weeks following TAA induction ( $0.053\pm 0.016$  copies per U6;  $n=3$ ;  $P=0.002$ ) when compared with sham-operated, nonaneurysm, control tissues ( $0.74\pm 0.099$  copies per U6;  $n=10$ ). (Figure 1B) Finally, linear regression analysis revealed an inverse correlation between aortic diameter and miR-133a copy number in aortic tissues ( $n=34$ ;  $r=-0.6356$ ;  $P<0.05$ ). (Figure 1C) As aortic diameter increased, miR-133a copy number was reduced.

### MiR-133a Was Decreased in Fibroblasts Isolated From TAA Tissue

For fibroblast specific studies, a separate cohort of mice underwent aneurysm induction. Descending thoracic aortic diameters were measured at the time of terminal surgery and determined to be

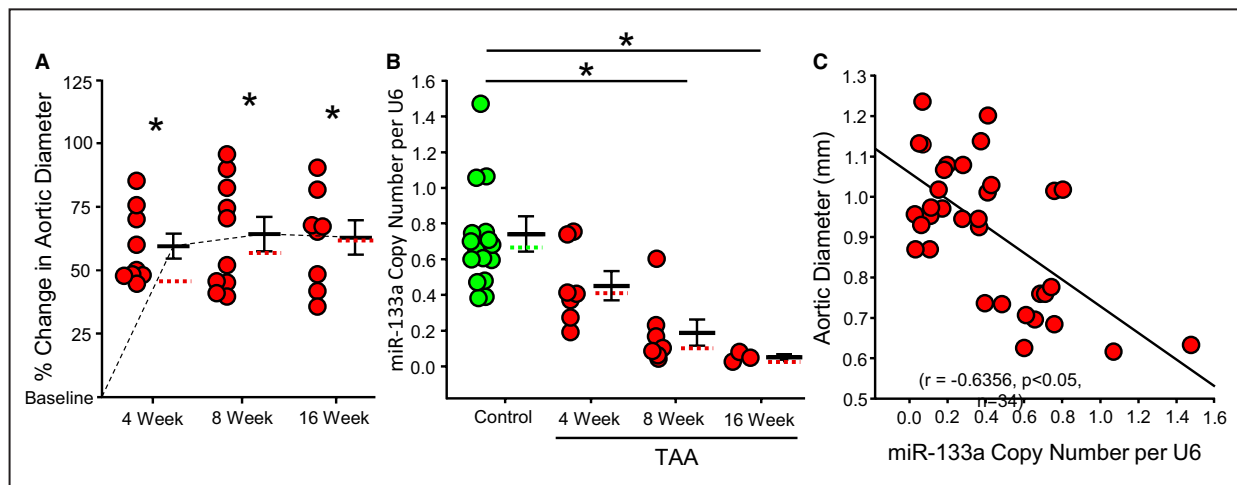


**Figure 1. MiR-133a is reduced in thoracic aortic aneurysm tissue.**

**A**, Percentage change in aortic diameter at 4 weeks ( $59.50\pm 4.90\%$ ,  $n=9$ ), 8 weeks ( $64.25\pm 6.77\%$ ,  $n=10$ ), and 16 weeks ( $62.89\pm 6.75\%$ ,  $n=8$ ) after aneurysm induction when compared with baseline diameter measurements. \*One-way ANOVA (Dunn's method) found differences between 4 weeks ( $P<0.001$ ), 8 weeks ( $P<0.001$ ), and 16 weeks ( $P<0.001$ ) after aneurysm induction vs baseline measurements. **B**, MiR-133a copy number in aortic tissue for sham-operated, nonaneurysmal control ( $0.74\pm 0.099$  copies per U6;  $n=10$ ) and 4 weeks ( $0.45\pm 0.082$  copies per U6;  $P=0.623$ ;  $n=7$ ), 8 weeks ( $0.19\pm 0.073$  copies per U6;  $n=7$ ), and 16 weeks ( $0.053\pm 0.016$  copies per U6;  $n=3$ ) after aneurysm induction. \*Kruskal-Wallis 1-way ANOVA on ranks found difference between 8 ( $P=0.004$ ) and 16 ( $P=0.002$ ) weeks vs control. Additionally, in a 1-way ANOVA all pairwise multiple comparison procedure (Tukey test), difference was detected between control vs 16 weeks ( $P=0.004$ ) and control vs 8 weeks ( $P=0.008$ ). **C**, Linear regression analysis demonstrating inverse correlation between aortic diameter (mm) and miR-133a copy number in aortic tissue ( $n=34$ ;  $r=-0.6356$ ;  $P<0.05$ ). In the vertical point plots, the solid line represents the mean, the upper and lower bars represent the standard error of the mean, and the dotted line represents the median.

701.22±17.24  $\mu\text{m}$  in the sham-operated, non-TAA, controls and 1019.49±41.82  $\mu\text{m}$  in the TAA group 4 weeks after induction, an  $\approx 50\%$  increase ( $n=10$ ;  $P<0.001$ ). (Figure 2A) Total RNA was extracted from a portion of the aortic tissues and used to

determine copy number of mRNA markers of myofibroblasts. Myh11 (myofibroblast marker) mRNA copy number was normalized to the fibroblast-specific DDR2 to account for any difference in fibroblast number. Myh11 mRNA copy number was

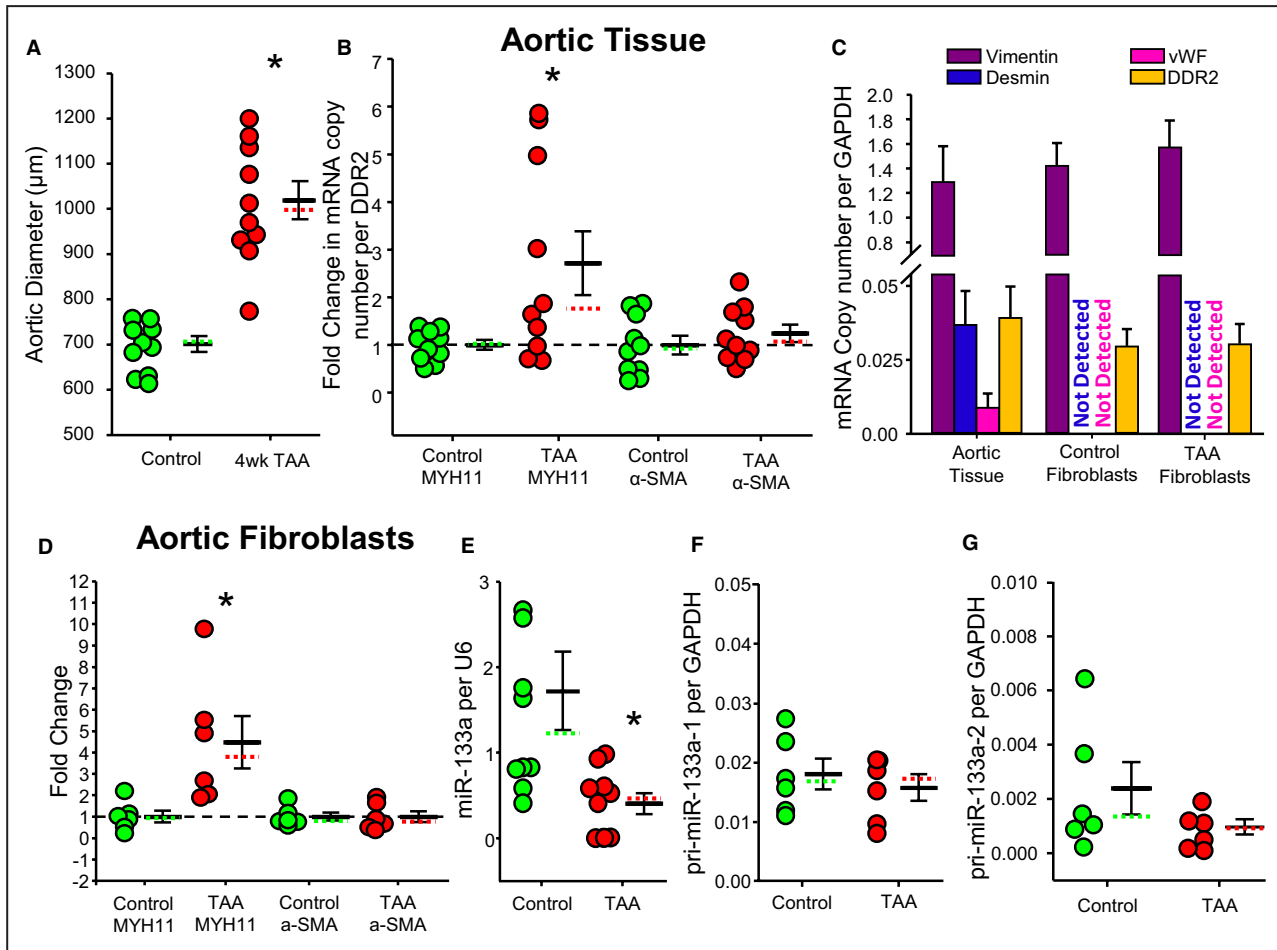


**Figure 2. MiR-133a was decreased in fibroblasts isolated from thoracic aortic aneurysm (TAA) tissue.**

**A**, Thoracic aortic diameter of sham-operated control (701.22±17.24  $\mu\text{m}$ ) and TAA (1019.49±41.82  $\mu\text{m}$ ) 4 weeks after induction surgery ( $n=10$ ). \*Student *t* test and Welch's *t* test found a difference between TAA vs control ( $P<0.001$ ). **B**, Fold change in smooth muscle myosin (Myh11) mRNA copy number per DDR2 copy number in control (1±0.10-fold) and TAA (2.71±0.67-fold) aortic tissue, as well as, alpha smooth muscle actin ( $\alpha$ -SMA) copy number in control (1±0.20-fold) and TAA (1.24±0.18-fold) tissue ( $n=10$ ). \*Mann-Whitney rank-sum test and Student *t* test found a difference between TAA vs control Myh11 copy number ( $P=0.045$ ). Student *t* test and Welch's *t* test did not find a difference between TAA  $\alpha$ -SMA vs control ( $P=0.378$ ). **C**, Detection of cell type-specific mRNAs in whole aortic tissue, and isolated fibroblasts from control and TAA aortae. Mesenchymal cell specific vimentin, smooth muscle cell-specific desmin, endothelial specific von Willebrand factor (vWF), and fibroblast specific DDR2 were all detected in whole aortic tissue homogenate, while only vimentin and discoidin domain receptor family, member 2 (DDR2) were present in the isolated control and TAA fibroblasts. No statistical test was performed. This is an analysis of presence or absence of cell specific mRNAs by droplet digital polymerase chain reaction (ddPCR) ( $n=10$ ). **D**, Fold change in Myh11 copy number in control (1±0.28-fold) and TAA (4.47±1.23-fold) fibroblasts and also  $\alpha$ -SMA copy number in control (1±0.187-fold) and TAA (1.003±0.26-fold) fibroblasts ( $n=6$ ). \*Student *t* test and Welch's *t* test found a difference between TAA and control Myh11 copy number ( $P=0.036$ ); however, no difference was found between TAA and control  $\alpha$ -SMA copy number ( $P=0.992$ ). **E**, MiR-133a copy number per U6 in control (1.72±0.46-fold) and TAA (0.41±0.12-fold) fibroblasts ( $n=10$ ). \*Mann-Whitney rank-sum test found a difference between TAA vs control aortic fibroblasts ( $P=0.007$ ). **F**, Pri-miR-133a-1 copy number per GAPDH in control (0.018±0.00259 copy per U6) and TAA (0.016±0.00224 copy per U6) fibroblasts ( $n=6$ ). Student *t* test and Welch's *t* test found no difference between control vs TAA fibroblasts ( $P=0.516$ ). **G**, Pri-miR-133a-2 copy number per GAPDH in control (2.40e-3±9.56e-4) and TAA (9.75e-4±2.83e-4) fibroblasts ( $n=6$ ). Student *t* test and Welch's *t* test found no differences between control vs TAA fibroblasts ( $P=0.205$ ). In the vertical point plots, the solid line represents the mean, the upper and lower bars represent the standard error of the mean, and the dotted line represents the median. In the vertical multibar graphs, the mean is represented by the bar, and the upper standard error of the mean is represented by the error bar.

increased in TAA tissue when compared with control ( $2.71 \pm 0.67$ -fold versus  $1.00 \pm 0.10$ -fold;  $n=10$ ;  $P=0.045$ ). Furthermore, alpha smooth muscle actin copy number remained unchanged in control and TAA tissue ( $1.00 \pm 0.20$ -fold versus  $1.24 \pm 0.18$ -fold;  $n=10$ ;  $P=0.378$ ) (Figure 2B). This gene expression profile is consistent with past reports and suggests the emergence of a myofibroblast population in TAA.<sup>2</sup>

With the remainder of the harvested aortic tissues, primary fibroblasts were isolated using an established outgrowth technique and maintained in culture.<sup>2</sup> Detection of cell type-specific mRNAs was performed by ddPCR in whole aortic tissue and the isolated fibroblast cultures from control and TAA aortas. Mesenchymal cell-specific vimentin, smooth muscle cell-specific desmin, endothelial-specific von Willebrand factor, and fibroblast-specific DDR2 were all detected in whole aortic tissue homogenate, while only vimentin and DDR2 mRNAs were present in the isolated control and TAA cells. Thus, successful isolation of DDR2-positive fibroblast cultures was achieved ( $n=10$ ) (Figure 2C). In the isolated fibroblasts, copy number of Myh11 mRNA was determined to be elevated in the fibroblasts derived from TAA tissue when compared with control ( $4.47 \pm 1.23$ -fold versus  $1.00 \pm 0.28$ -fold;  $n=6$ ;  $P=0.036$ ). Furthermore, no change was detected in alpha smooth muscle

actin copy number in control versus TAA fibroblasts ( $1.00 \pm 0.187$ -fold versus  $1.003 \pm 0.26$ -fold;  $n=6$ ;  $P=0.992$ ) (Figure 2D). Most importantly, miR-133a copy number was significantly reduced in TAA fibroblasts when compared with control ( $0.41 \pm 0.12$  versus  $1.72 \pm 0.46$  copy per U6;  $n=10$ ;  $P=0.007$ ) (Figure 2E). Interestingly, no differences were detected in copy numbers of primary miR-133a in control versus TAA fibroblasts (primary miR-133a-1:  $0.018 \pm 0.00259$  versus  $0.016 \pm 0.00224$  copy per GAPDH;  $n=6$ ;  $P=0.516$ ) (Figure 2F); primary miR-133a-2:  $2.40 \times 10^{-3} \pm 9.56 \times 10^{-4}$  versus  $9.75 \times 10^{-4} \pm 2.83 \times 10^{-4}$  copy per GAPDH,  $n=6$ ,  $P=0.205$ ) (Figure 2G), suggesting regulation of mature levels after transcription.

### Phenotype Was Altered in Fibroblasts Isolated From TAA Tissue

Phenotype was compared between control and TAA fibroblasts. Migration was increased in TAA fibroblasts when compared with control ( $0.62 \pm 0.041\%$ ;  $n=9$  versus  $0.47 \pm 0.038\%$ ,  $n=10$ ;  $P=0.013$ ) (Figure 3A). Representative images of the migration assay are included in Figure S2. Adhesion to a growth surface was reduced in TAA fibroblasts when compared with control ( $-0.85 \pm 0.018$ -fold versus  $-0.77 \pm 0.022$ -fold;  $n=10$ ;  $P=0.009$ ) (Figure 3B). Finally, contraction of a collagen disk was increased with TAA fibroblasts when compared

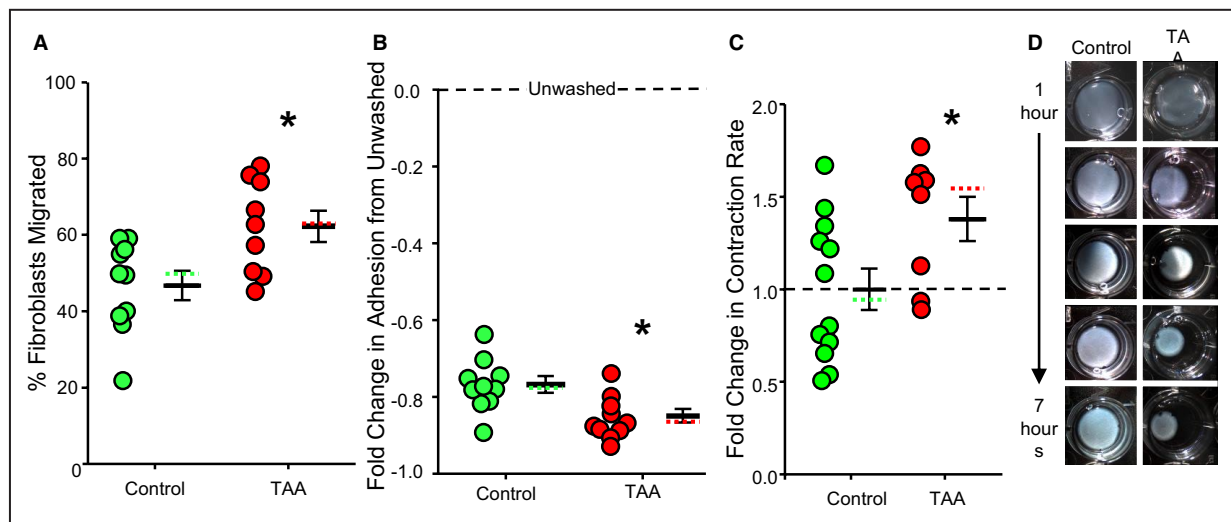


**Figure 3. Phenotype was altered in fibroblasts isolated from thoracic aortic aneurysm (TAA) tissue.**

**A**, Migration of aortic fibroblasts as determined by transwell assay. Displayed are the percent of total cells migrated through an 8- $\mu$ m porous membrane following 24-hour incubation of control ( $0.47 \pm 0.038\%$ ,  $n=10$ ) and TAA ( $0.62 \pm 0.041\%$ ,  $n=9$ ) fibroblasts. \*Student *t* test and Welch's *t* test found differences between TAA vs control fibroblasts ( $P=0.013$ ). **B**, Adhesion of aortic fibroblasts following repeat washes in an automated plate washer. Displayed is a fold change in cell count compared with unwashed in control ( $-0.77 \pm 0.022$ -fold) and TAA ( $-0.85 \pm 0.018$ -fold) fibroblasts ( $n=10$ ). \*Student *t* test and Welch's *t* test found a difference between 4-week TAA vs control fibroblasts ( $P=0.009$ ). **C**, Fold change in contraction rate of a collagen disk seeded with control ( $1.00 \pm 0.39$ -fold,  $n=12$ ) or TAA ( $1.38 \pm 0.34$ -fold,  $n=8$ ) fibroblasts. \*Student *t* test and Welch's *t* test found a difference in contraction rate between control and TAA fibroblasts ( $P=0.034$ ). **D**, Representative images of collagen disks seeded with control or TAA fibroblasts over 7 hours (images taken at 1, 3, 5, 6, and 7 hours from collagen polymerization). In the vertical point plots, the solid line represents the mean, the upper and lower bars represent the standard error of the mean, and the dotted line represents the median.



with control (1.38±0.34-fold; n=8 versus 1.00±0.39-fold; n=12;  $P=0.034$ ) (Figure 3C). This phenotypic profile is consistent with that of the highly migratory and

contractile myofibroblast. Figure 3D shows representative images of the collagen disks seeded with fibroblasts over the 7-hour time course of the experiment.

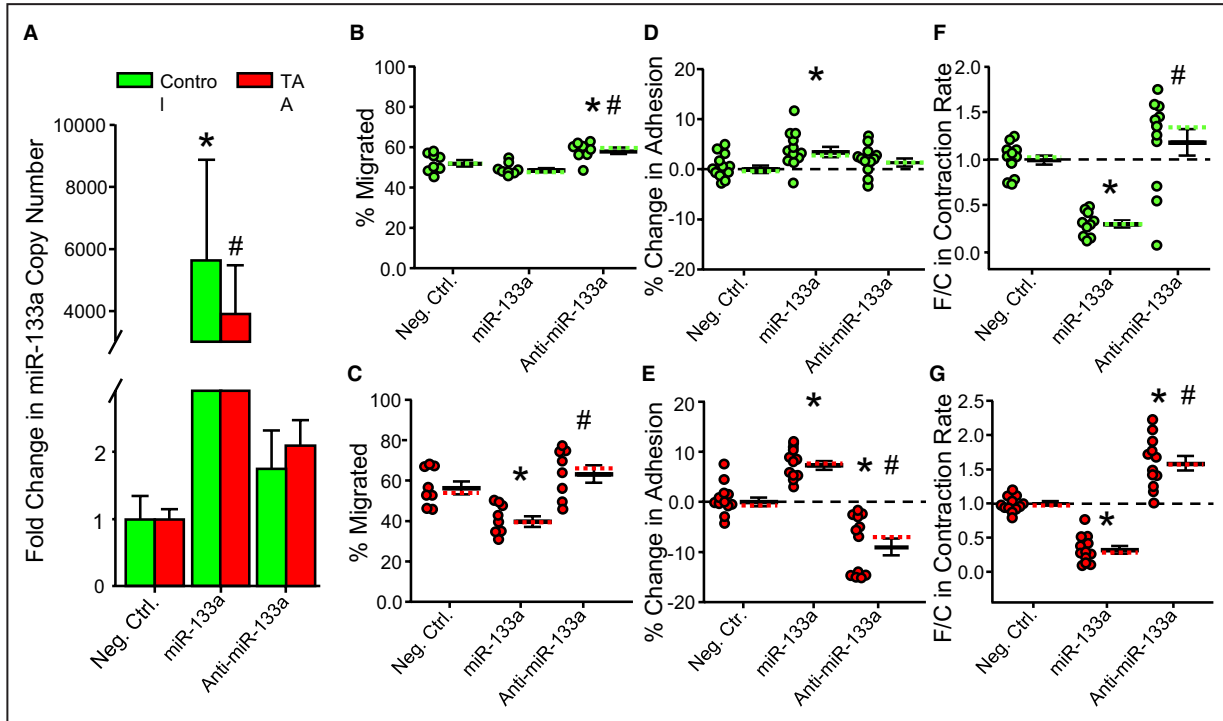


**Figure 4. MiR-133a modulates aortic fibroblast phenotype.**

**A**, Fold change in control (green) and TAA (red) fibroblast miR-133a copy number following transfection with the negative control microRNA mimic (Neg. Ctrl.) (control: 1.00±0.35-fold; TAA: 1.00±0.15-fold; n=8), miR-133a mimic (control: 5637.49±3247.71-fold,  $P<0.001$ , n=8; TAA: 3905.97±1570.75-fold,  $P<0.001$ , n=7), and anti-miR-133a oligonucleotide (control: 1.75±0.57-fold,  $P=0.495$ ; TAA: 2.09±0.37-fold,  $P=0.421$ ; n=8). \*, # Kruskal-Wallis 1-way ANOVA on ranks with Tukey test for post hoc analysis found differences between miR-133a copy number in both control and TAA fibroblasts transfected with the miR-133a mimic vs fibroblasts transfected with the negative control mimic. **B**, Percentage of total control fibroblasts migrated through an 8µm porous membrane following transfection with the negative control microRNA mimic (0.52±0.017%), miR-133a mimic (0.49±0.010%), and anti-miR-133a oligonucleotide (0.58±0.016%) (n=8). \*One-way ANOVA, multiple comparisons vs control group (Bonferroni *t* test) found a difference between anti-miR-133a oligonucleotide vs negative control mimic ( $P<0.012$ ). #One-way ANOVA, all pairwise multiple comparison procedure (Tukey test) found a difference between anti-miR-133a vs miR-133a ( $P<0.001$ ). **C**, Percent of total TAA fibroblasts migrated through an 8-µm porous membrane following transfection with the negative control microRNA mimic (0.56±0.034%), miR-133a mimic (0.40±0.026%), and anti-miR-133a oligonucleotide (0.63±0.043%) (n=8). \*One-way ANOVA, multiple comparisons vs control group (Bonferroni *t* test) found difference between miR-133a mimic vs negative control mimic ( $P=0.006$ ). #One-way ANOVA, multiple comparison procedure (Tukey test) vs miR-133a mimic found difference between anti-miR-133a vs miR-133a ( $P<0.001$ ). **D**, Percent change in control fibroblast adhesion following transfection with the negative control mimic (0.00±0.7%), miR-133a mimic (3.4±1.0%), and anti-miR-133a oligonucleotide (1.3±0.08%) (n=12). \*One-way ANOVA, multiple comparisons vs control group (Bonferroni *t* test) found difference between miR-133a mimic vs negative control mimic ( $P=0.016$ ). **E**, Percentage change in TAA fibroblast adhesion following transfection with the negative control mimic (0.00±0.009%), miR-133a mimic (7.3±0.08%), and anti-miR-133a oligonucleotide (-9.0±0.17%) (n=12). \*One-way ANOVA, multiple comparisons vs control group (Dunn's method) found differences between miR-133a vs negative control ( $P=0.016$ ) and anti-miR-133a vs negative control ( $P=0.016$ ). #One-way ANOVA, multiple comparisons vs miR-133a group (Dunn's method) found difference between anti-miR-133a vs miR-133a ( $P<0.001$ ). **F**, Fold change (F/C) in contraction rate of a collagen disk seeded with control fibroblasts transfected with negative control mimic (1.0±0.049, n=12), miR-133a mimic (0.30±0.042, n=10), and anti-miR-133a oligonucleotide (1.18±0.14, n=12). \*One-way ANOVA, multiple comparisons vs control group (Dunn's method) found differences between miR-133a vs negative control ( $P=0.006$ ). #One-way ANOVA, multiple comparisons vs miR-133a group (Dunn's method) found differences between anti-miR-133a vs miR-133a ( $P<0.001$ ). **G**, F/C in contraction rate of a collagen disk seeded with TAA fibroblasts transfected with negative control mimic (1.00±0.033, n=12), miR-133a mimic (0.32±0.058, n=10), and anti-miR-133a oligonucleotide (1.59±0.11; n=12). \*One-way ANOVA, multiple comparisons vs control group (Dunn's method) found differences between anti-miR-133a vs negative control ( $P=0.021$ ) and between miR-133a vs negative control ( $P=0.007$ ). #One-way ANOVA, multiple comparisons vs miR-133a group (Dunn's method) found difference found between miR-133a vs negative control ( $P<0.001$ ). In the vertical point plots, the solid line represents the mean, the upper and lower bars represent the standard error of the mean, and the dotted line represents the median. In **D** through **G**, the dashed line represents referent control levels.

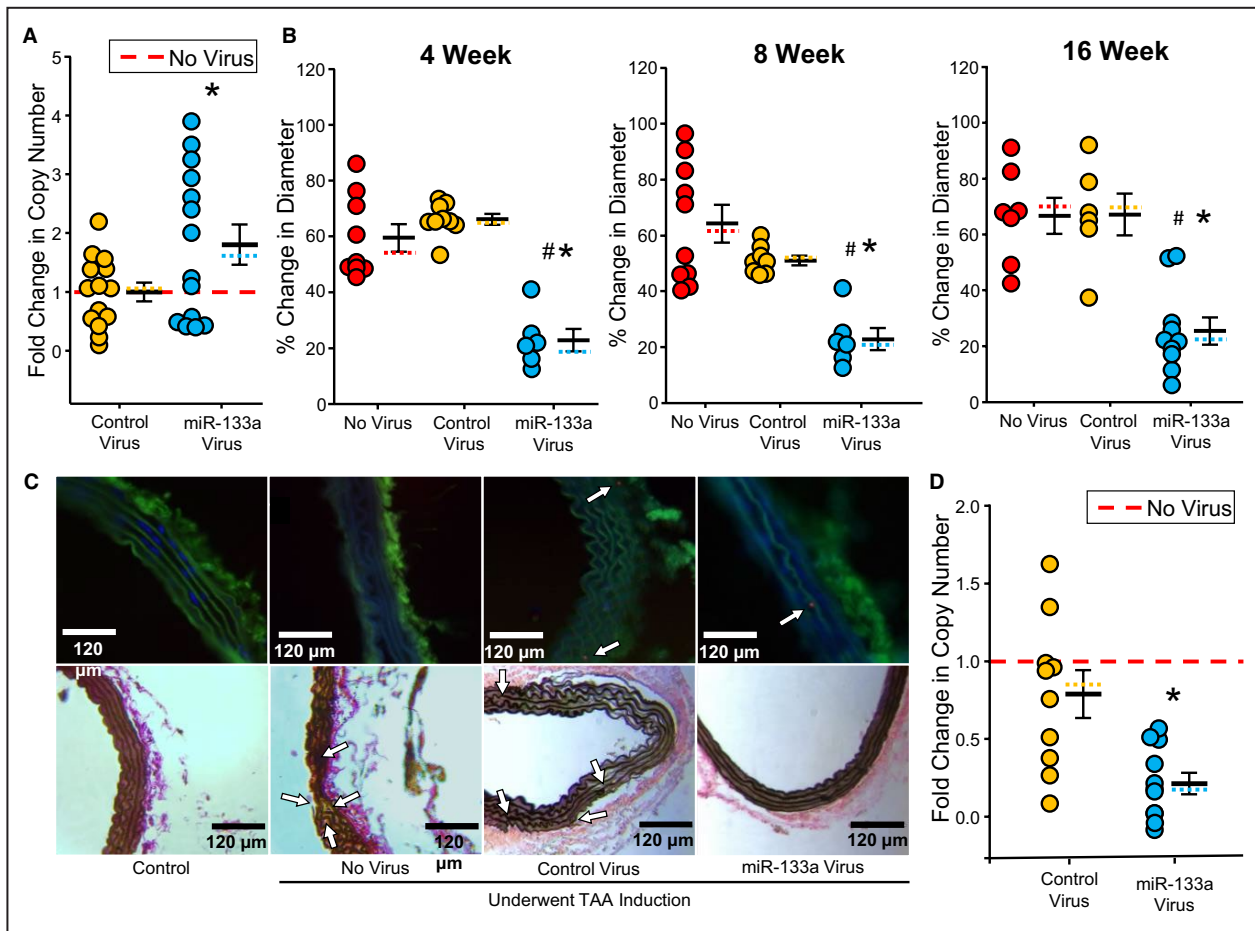


**Figure 5. MiR-133a attenuates the development of thoracic aortic aneurysms (TAA) in mice.**

**A**, Fold change in aortic tissue miR-133a copy number following TAA induction in mice transfected with either the control virus ( $1.00 \pm 0.16$ -fold) or the miR-133a over expression virus ( $1.81 \pm 0.34$ -fold) compared with nontransfected mice with TAA (red dashed line) ( $n=14$ ). \*Student *t* test and Welch's *t* test found a difference between miR-133a virus vs control virus ( $P=0.048$ ). **B**, Percentage change in aortic diameter in nontransfected (no virus) and transfected mice with the control virus, and miR-133a virus 4 weeks (no virus:  $55.70 \pm 5.80\%$ ,  $n=9$ ; control virus:  $65.95 \pm 1.97\%$ ,  $n=9$ ; miR-133a virus:  $24.64 \pm 2.19\%$ ,  $n=9$ ), 8 weeks (no virus:  $0.64 \pm 0.07\%$ ,  $n=10$ ; control virus:  $0.49 \pm 0.03\%$ ,  $n=9$ ; miR-133a virus:  $0.23 \pm 0.04\%$ ,  $n=6$ ), and 16 weeks (no virus:  $0.63 \pm 0.07\%$ ,  $n=8$ ; control virus:  $0.62 \pm 0.08\%$ ,  $n=7$ ; miR-133a virus:  $0.25 \pm 0.05\%$ ,  $n=10$ ) after aneurysm induction. \*One-way ANOVA, multiple comparisons vs control group (Bonferroni *t* test) found difference between miR-133a virus vs no virus at 4 ( $P<0.001$ ) and 16 ( $P<0.001$ ) weeks. No difference was found between control virus vs no virus at 4 ( $P=0.359$ ) or 16 ( $P=1$ ) weeks. One-way ANOVA, multiple comparisons vs control group (Dunn's method) found difference between miR-133a virus vs no virus at 8 ( $P<0.001$ ) weeks. No difference was found between control virus vs no virus at 8 weeks ( $P=0.761$ ). #One-way ANOVA, all pairwise multiple comparison procedure (Tukey test) found differences between miR-133a virus vs control virus at 4 weeks ( $P<0.001$ ) and 16 weeks ( $P=0.001$ ), and no difference between no virus vs control virus at 4 ( $P=0.366$ ) or 16 ( $P=0.999$ ) weeks. One-way ANOVA, multiple comparisons vs control group (Dunn's method) found a difference between miR-133a virus vs control virus at 8 weeks ( $P=0.02$ ) and no difference between no virus vs control virus at 8 weeks ( $P=1$ ). **C**, Immunofluorescence (top) and modified Verhoeff–Van Gieson stain elastic stain (bottom) of non-TAA control and nontransfected (no virus) and transfected mice with the control virus, and miR-133a virus aortic sections 16 weeks following the TAA induction procedure. In the immunofluorescent images, elastin is seen as green autofluorescence, nuclei are stained blue with DAPI, and red is a primary antibody to the green fluorescent protein conjugated with a secondary antibody labeled with a red Alexafluor. White arrows indicate transduced cells and elastin breaks. In the vertical point plots, the solid line represents the mean, the upper and lower bars represent the standard error of the mean, and the dotted line represents the median. **D**, Fold change in aortic tissue Myh11 copy number per DDR2 copy following TAA induction in mice transfected with either the control virus ( $0.79 \pm 0.15$ -fold) or the miR-133a overexpression virus ( $0.33 \pm 0.07$ -fold) compared with nontransfected mice with TAA (red dashed line) ( $n=11$ ). \*Student *t* test and Welch's *t* test found a difference between miR-133a virus vs control virus ( $P=0.018$ ).

### MiR-133a Modulated Aortic Fibroblast Phenotype

To investigate the effects of miR-133a on cellular phenotype, control and TAA fibroblasts were transfected

with either a nontargeting control microRNA mimic as a negative control, a miR-133a mimic to increase cellular levels, or an anti-miR-133a oligonucleotide for suppression of endogenous miR-133a. Following

transfection, the copy number of miR-133a was quantified in the control and TAA fibroblasts. Results confirmed that transfection of the miR-133a mimic increased cellular levels of miR-133a in control and TAA fibroblasts (control:  $1.00\pm 0.35$ -fold and TAA:  $1.00\pm 0.15$ -fold transfected with the negative control mimic; control:  $5637.49\pm 3247.71$ -fold;  $P<0.001$ ;  $n=8$  and TAA:  $3905.97\pm 1570.75$ -fold;  $P<0.001$ ;  $n=7$  when transfected with the miR-133a mimic). As anticipated, the anti-miR-133a had no effect on mature miR-133a copy number in control nor TAA fibroblasts (control:  $1.75\pm 0.57$ -fold;  $P=0.495$ ; and TAA:  $2.09\pm 0.37$ -fold;  $P=0.421$ ;  $n=8$ ) (Figure 4A).

Following overexpression and knockdown of miR-133a, cellular phenotype was measured in control and TAA fibroblasts. When control fibroblasts were treated with miR-133a, there was a slight reduction in migration; however, this did not reach statistical significance. Conversely, when control fibroblasts were transfected with the anti-miR-133a oligonucleotide, migration was significantly increased (negative control microRNA mimic:  $0.52\pm 0.017\%$ ; miR-133a mimic  $0.49\pm 0.010\%$ ; and anti-miR-133a  $0.58\pm 0.016\%$ ;  $n=8$ ,  $P=0.012$  anti-miR-133a versus negative control) (Figure 4B). Alternatively, when TAA fibroblasts were treated with miR-133a, there was a significant reduction in migration, while TAA fibroblasts transfected with the anti-miR-133a did not have a significant increase in migration (negative control microRNA mimic:  $0.56\pm 0.034\%$ ; miR-133a mimic:  $0.40\pm 0.026\%$ ; anti-miR-133a oligonucleotide:  $0.63\pm 0.043\%$ ;  $n=8$ ,  $P=0.006$  miR-133a versus negative control) (Figure 4C).

Adhesion was increased in control fibroblasts transfected with the miR-133a mimic, while no change was observed in control fibroblasts treated with the anti-miR-133a oligonucleotide (negative control:  $0.00\pm 0.7\%$ ; miR-133a mimic:  $3.4\pm 1.0\%$ ; anti-miR-133a:  $1.3\pm 0.08\%$ ;  $n=12$ ;  $P=0.016$  miR-133a versus negative control) (Figure 4D). Conversely, in TAA fibroblasts, adhesion was increased following miR-133a transfection, while reduced when treated with the anti-miR-133a oligonucleotide (negative control:  $0.00\pm 0.009\%$ ; miR-133a mimic:  $7.3\pm 0.08\%$ ; anti-miR-133a:  $-9.0\pm 0.17$ ;  $n=12$ ;  $P=0.016$  miR-133a versus negative control and  $P<0.001$  anti-miR-133a versus negative control) (Figure 4E).

Fold change in contraction rate was significantly reduced in control fibroblasts treated with the miR-133a mimic, while transfection with the anti-miR-133a oligonucleotide resulted in a moderate increase (negative control microRNA mimic:  $1.0\pm 0.049$ ; miR-133a mimic:  $0.30\pm 0.042$ ; anti-miR-133a:  $1.18\pm 0.14$ ;  $n=12$ ;  $P=0.006$  miR-133a versus negative control) (Figure 4F). Conversely, when TAA fibroblasts were treated with miR-133a mimic, contraction was

reduced and treatment with the anti-miR-133a oligonucleotide increased contraction significantly (negative control mimic:  $1.00\pm 0.033$ ; miR-133a mimic:  $0.32\pm 0.058$ ; anti-miR-133a oligonucleotide:  $1.59\pm 0.11$ ;  $n=12$ ;  $P=0.021$  miR-133a versus negative control and  $P=0.007$  anti-miR-133a versus negative control) (Figure 4G).

## MiR-133a Attenuates the Development of TAA in Mice

To demonstrate the impact of miR-133a overexpression on aneurysm development, 3 cohorts of mice underwent TAA induction. The following day, one group received a control, nontargeting, scrambled sequence virus, while another group was given the miR-133a overexpression virus. At the time of terminal surgery, miR-133a levels were confirmed to be increased in the thoracic aorta of mice that received the miR-133a overexpression virus versus the nontransfected mice with TAA ( $1.81\pm 0.34$ -fold versus  $1.00\pm 0.16$ ;  $n=14$ ;  $P=0.048$ ). Furthermore, no difference in miR-133a copy number was detected between mice with TAA transfected with the control virus (vehicle control) versus the nontransfected mice with TAA (Figure 5A). A true aneurysm, defined as a  $>50\%$  increase in aortic diameter, was confirmed in mice that did not receive virus and those that received the control virus at 4, 8, and 16 weeks following induction. Furthermore, no differences were detected in diameter measurements between the no-virus and control-virus groups. Conversely, treatment with the miR-133a virus attenuated aneurysm development at 4, 8, and 16 weeks following induction (4 weeks: no virus:  $55.70\pm 5.80\%$ ,  $n=9$ ; control virus:  $65.95\pm 1.97\%$ ,  $n=9$ ; miR-133a virus:  $24.64\pm 2.19\%$ ,  $n=9$ ;  $P<0.001$  versus no virus and control virus) (8 weeks: no virus:  $64\pm 7\%$ ,  $n=10$ ; control virus:  $49\pm 3\%$ ,  $n=9$ ; miR-133a virus:  $23\pm 4\%$ ,  $n=6$ ;  $P<0.001$  versus no virus and control virus) (16 weeks: no virus:  $63\pm 7\%$ ,  $n=8$ ; control virus:  $62\pm 8\%$ ,  $n=7$ ; miR-133a virus:  $25\pm 5\%$ ,  $n=10$ ;  $P<0.001$  versus no virus and control virus) (Figure 5B).

Both control virus and the miR-133a overexpression virus coexpress the green fluorescent protein. Accordingly, tissue sections from each group were obtained 16 weeks following TAA induction and subjected to green fluorescent protein-specific primary immunohistochemistry followed by a red fluorescently labeled secondary antibody. Negative signal was observed in the non-TAA (control) and TAA with no-virus sections, while positive red signal was detected in both control-virus and miR-133a overexpression virus tissues. Combined, this confirmed successful viral transduction of aortic tissue and sustained gene expression throughout the 16-week time course of the study (Figure 5C, top). Additional fluorescent images

are available in Figure S3. Tissue sections were also stained with a modified Verhoeff's stain to confirm elastic degeneration within the media of the TAA tissues. Conversely, the elastin filaments in the miR-133a overexpression group appear to be largely intact and similar in structure to the nonvirus control sections (Figure 5C, bottom).

Finally, total RNA was extracted from a portion of the TAA tissues and used to determine copy number of an mRNA marker of myofibroblasts. Myh11 mRNA copy number was normalized to DDR2 as previously described to account for differences in fibroblast number. No difference was detected between the no-virus and control-virus groups, while Myh11 mRNA copy number was significantly reduced in aortic tissues from mice that received the miR-133a overexpression virus. Thus, suggesting successful prevention of myofibroblast population expansion. ( $1.00\pm 0.15$  versus  $0.33\pm 0.07$ -fold;  $n=10$ ;  $P=0.012$ ) (Figure 5D). Consistent with control tissues, alpha smooth muscle actin remained unchanged (Figure S4).

### MiR-133a Directly Regulates Furin Translation

To identify an underlying molecular pathway involved with miR-133a and attenuation of aneurysm development, a bioinformatics approach was taken to uncover potential targets involved with extracellular matrix remodeling. A TargetScan analysis, which is a widely used predictor of microRNA targets, identified a putative binding site in the 3'UTR of the pro-protein convertase furin, a molecule highly involved with ECM remodeling through activation of the membrane type matrix metalloproteinases as well as release of latent ECM-bound growth factors.<sup>20–22</sup> Furthermore, this sequence and surrounding regions are highly conserved across multiple (>42) species. Additionally, 5 online bioinformatics tools for microRNA target recognition (MicroCosm Targets Version 5; DIANA; PITA; RNA22; and RNAhybrid) identified miR-133a as a top candidate at the same seed region sequence, GACCA, of the furin mRNA transcript (Figure 6A). Furin abundance was confirmed to be elevated in isolated murine TAA fibroblasts when compared with control fibroblasts ( $1.89\pm 0.20$ -fold versus  $1.00\pm 0.05$ -fold;  $n=15, 12$ ;  $P<0.001$ ) (Figure 6B). Complete uncropped images of the western blots are included in Figure S5.

To confirm a direct interaction between miR-133a and the furin mRNA transcript, several luciferase reporter constructs were employed. The first contained the native furin 3'UTR sequence (NM\_001289823.2), while another had only the GACCA sequence exchanged for CUGGU by site directed mutagenesis (mut-furin, illustrated in Figure 6A). For further controls, a random sequence 3'UTR vector, which did not contain GACCA, and another construct with no 3'UTR were

included. Luminescence production was quantified following cotransfection with either a miR-133a mimic or a negative control (non-GACCA targeting) microRNA mimic in HT1080 cells. Results demonstrate a decrease in luminescence only in the cells cotransfected with the native furin 3'UTR construct and the miR-133a mimic ( $0.62\pm 0.10$ -fold versus  $1.00\pm 0.10$ -fold;  $n=4$ ;  $P=0.024$ ) (Figure 6C). Thus, miR-133a directly targets the consensus sequence GACCA, located in the furin 3'UTR.

To determine if miR-133a modulates furin translation in vitro, murine control and TAA aortic fibroblasts were transfected with either a nontargeting control microRNA mimic as a negative control, a miR-133a mimic to increase cellular levels, or an anti-miR-133a oligonucleotide for suppression of endogenous miR-133a. In control fibroblasts, miR-133a did not further reduce furin abundance when compared with the negative control ( $0.69\pm 0.14$ -fold versus  $1.00\pm 0.14$ -fold;  $n=6$ ;  $P=0.399$ ). Conversely, furin abundance in control fibroblasts transfected with the anti-miR-133a oligonucleotide was significantly increased when compared with the fibroblasts treated with the negative control microRNA mimic ( $1.59\pm 0.21$ -fold versus  $1.00\pm 0.14$ -fold;  $n=6$ ;  $P=0.04$ ) (Figure 6D). Contrariwise, in TAA fibroblasts, miR-133a significantly reduced furin abundance when compared with the negative control ( $0.61\pm 0.07$ -fold versus  $1.00\pm 0.12$ -fold;  $n=6$ ;  $P=0.04$ ), while furin abundance in TAA fibroblasts transfected with the anti-miR-133a oligonucleotide was not further increased ( $1.16\pm 0.11$ -fold versus  $1.00\pm 0.12$ -fold;  $n=6$ ;  $P=0.75$ ) (Figure 6E).

### MiR-133a Overexpression Modulates Furin in Aortic Tissue

The downstream effects of miR-133a overexpression were investigated in vivo. (pathway illustrated in Figure 7A) For this, a portion of aortic tissue was used from the 3 cohorts of mice that underwent TAA induction and compared with non-TAA, control aortic tissues. One group received aneurysm induction with no virus injection, another received a control, nontargeting, scrambled sequence virus, while the third received the miR-133a overexpression virus. Following aneurysm formation, furin abundance was determined to be elevated in TAA when compared with non-TAA control tissue ( $2.54\pm 0.31$ -fold versus  $1.00\pm 0.06$ -fold;  $n=12$ ;  $P<0.001$ ). As anticipated, no difference in furin abundance was detected between the no-virus and control-virus groups with TAA. However, overexpression of miR-133a prevented an increase in furin levels following TAA induction in mice, and there was no difference when compared with non-TAA control levels ( $1.17\pm 0.15$ -fold versus  $1.00\pm 0.06$ -fold;  $n=12$ ;  $P=1$ ) (Figure 7B).

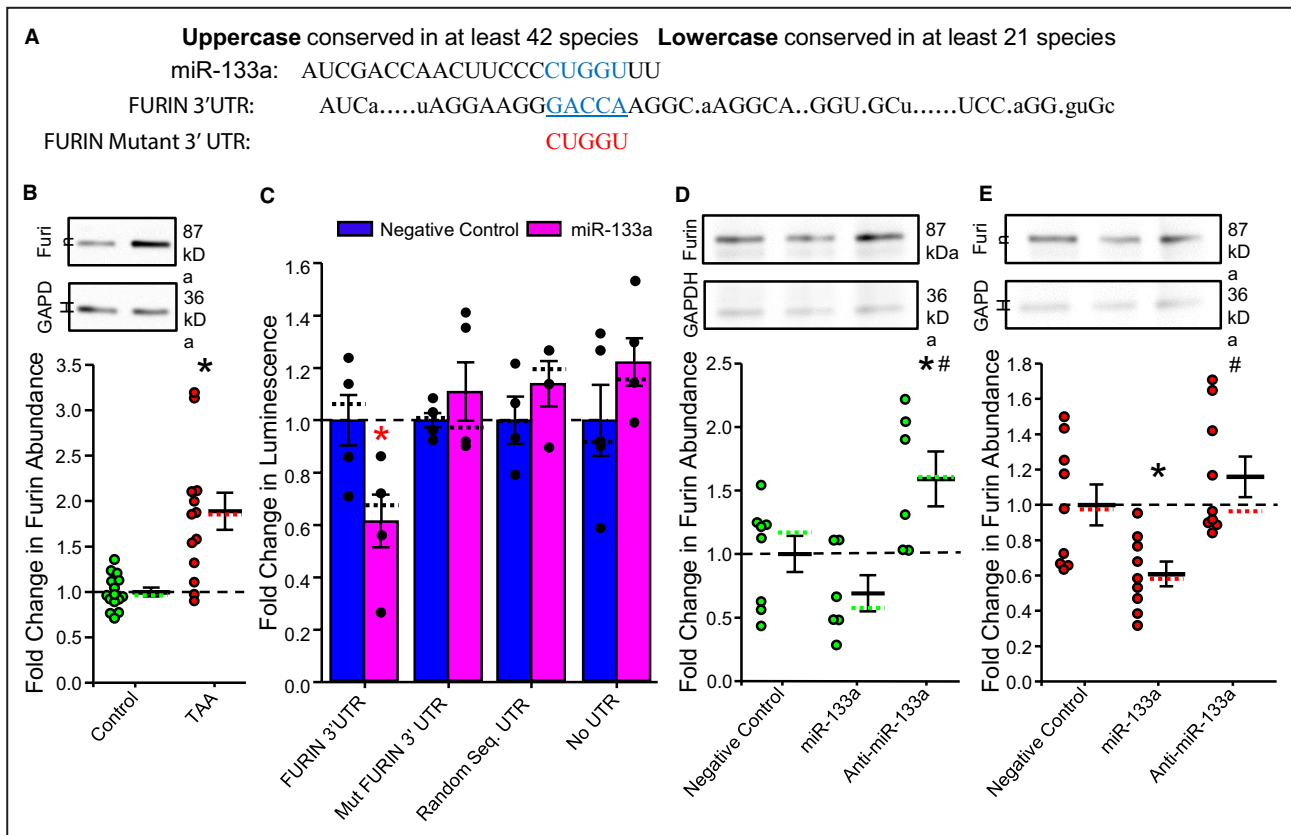


**Figure 6. MiR-133a directly regulates furin translation.**

**A**, Sequence alignment between the mature miR-133a transcript (accession: MIMAT0000427) with the conserved sequence region of the furin 3' untranslated region (UTR). Transcript in uppercase is conserved in at least 42 species, and transcript in lowercase is conserved in at least 21 species (TargetScan 7.2). Below is the gene mutation sequence introduced in the 3'UTR of the mutant furin reporter plasmid for confirmation of direct targeting. **B**, Furin is elevated in thoracic aortic aneurysm (TAA) fibroblasts. Displayed is the fold change in furin abundance of control ( $1.0 \pm 0.05$ -fold,  $n=15$ ) and TAA ( $1.89 \pm 0.20$ -fold,  $P < 0.001$ ,  $n=12$ ) fibroblasts with representative immunoblot above. \*Mann-Whitney rank-sum test found difference between TAA vs control ( $P < 0.001$ ). **C**, MiR-133a directly targets the GACCA consensus sequence located in the furin 3'UTR. Displayed is the fold change in luminescence following cotransfection of HT1080 cells with the following 3'UTR luciferase reporter constructs and either a nontargeting negative control microRNA mimic or miR-133a: the wild-type furin 3'UTR construct cotransfected with either the negative control ( $1.00 \pm 0.10$ -fold) or miR-133a mimic ( $0.62 \pm 0.10$ -fold); the mutated furin 3'UTR (with GACCA replace with CUGGU by site-directed mutagenesis) construct cotransfected with the negative control ( $1.00 \pm 0.03$ -fold) and miR-133a ( $1.12 \pm 0.11$ ); a random sequence 3'UTR construct (confirmed to not contain GACCA) with the negative control ( $1.00 \pm 0.09$ ) and miR-133a ( $1.14 \pm 0.09$ ), and a positive control construct (which contains no 3'UTR [no UTR]) cotransfected with the negative control ( $1.00 \pm 0.14$ -fold) or miR-133a ( $1.22 \pm 0.09$ -fold) ( $n=5$ ). \*Student *t* test and Welch's *t* test found differences in luminescence between the furin 3'UTR transfected with the miR-133a mimic vs when transfected with the nontargeting, negative control, microRNA mimic ( $P=0.024$ ). **D**, Furin abundance in control fibroblasts following transfection with the negative control microRNA mimic ( $1.0 \pm 0.14$ ;  $n=8$ ), miR-133a mimic ( $0.609 \pm 0.070$ ;  $P < 0.399$ ;  $n=6$ ), and anti-miR-133a oligonucleotide ( $1.59 \pm 0.22$ ;  $n=6$ ) with representative immunoblot above. \*One-way ANOVA, multiple comparisons vs control group (Bonferroni *t* test) found difference between anti-miR-133a vs negative control ( $P=0.041$ ). #One-way ANOVA, all pairwise multiple comparison procedure (Tukey test) found difference between anti-miR-133a vs miR-133a ( $P=0.006$ ). **E**, Furin abundance in TAA fibroblasts following transfection with the negative control microRNA mimic ( $1.00 \pm 0.116$ ;  $n=9$ ), miR-133a mimic ( $0.609 \pm 0.070$ ;  $P=0.041$ ;  $n=9$ ), and anti-miR-133a oligonucleotide ( $1.16 \pm 0.11$ ;  $n=9$ ) with representative immunoblot above. \*One-way ANOVA, multiple comparisons vs control group (Dunn's method) found difference between miR-133a and negative control group ( $P=0.054$ ). #One-way ANOVA, multiple comparisons vs miR-133a group (Dunn's method) found difference between anti-miR-133a vs miR-133a ( $P=0.004$ ). In **D**, the bar height represents the mean, the upper and lower bars represent the standard error of the mean, and the dotted line represents the median. In the vertical point plots, the solid line represents the mean, the upper and lower bars represent the standard error of the mean, and the dotted line represents the median.

It is well established that the pro-protein convertase, furin, activates the MT1-MMP intracellularly by removal of a pro-domain.<sup>20,23</sup> Therefore, the proteolytically active, 64-kDa form of MT1-MMP was measured in the aortic tissues. Following aneurysm

formation, active MT1-MMP abundance was determined to be elevated in TAA when compared with non-TAA control tissue ( $1.38 \pm 0.11$ -fold versus  $1.00 \pm 0.07$ -fold;  $n=12$ ;  $P=0.005$ ). As anticipated, no difference in active MT1-MMP was detected

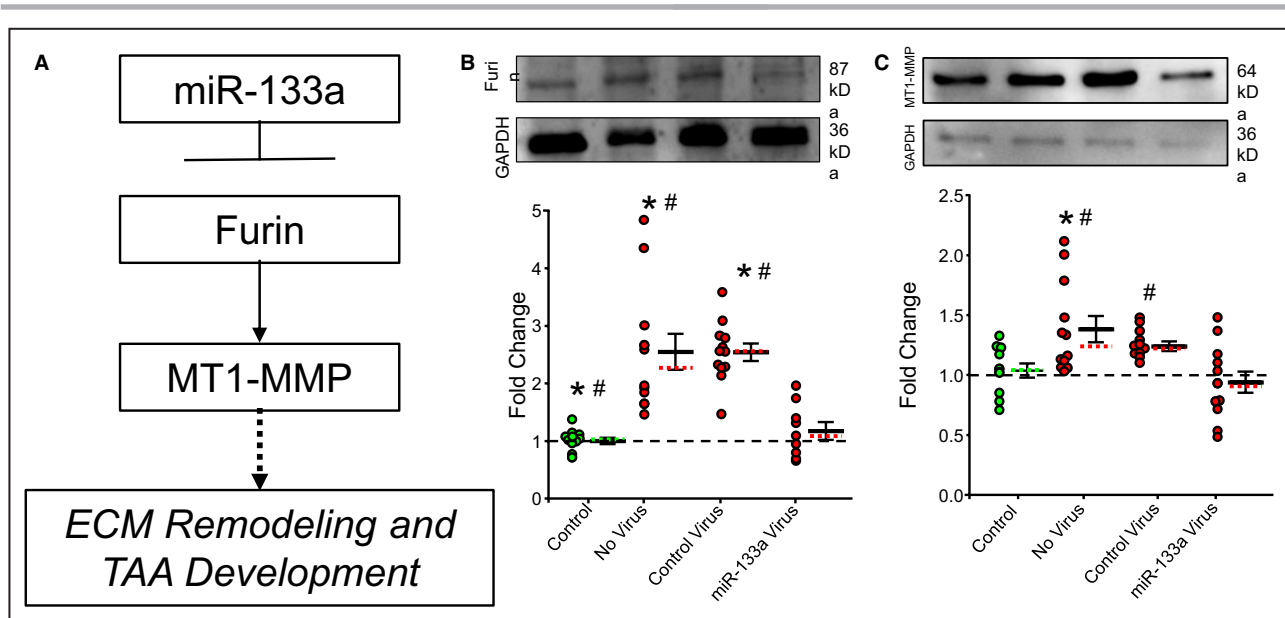


**Figure 7. MiR-133a overexpression modulates furin in aortic tissue.**

**A**, Proposed pathway of miR-133a regulation of extracellular matrix (ECM) remodeling. **B**, representative western blot and fold change in furin abundance in control tissue ( $1 \pm 0.055$ ,  $n=12$ ) and thoracic aortic aneurysms (TAA) tissue transfected with no virus ( $2.5 \pm 0.31$ ,  $n=12$ ), control virus ( $2.54 \pm 0.15$ ,  $n=12$ ), and miR-133a virus ( $1.18 \pm 0.15$ ,  $P=1$ ,  $n=9$ ). \*One-way ANOVA, multiple comparisons vs control group (Dunn's method) found differences between control group vs no virus ( $P < 0.001$ ) and vs control virus ( $P < 0.001$ ). #One-way ANOVA, multiple comparisons vs miR-133a group (Dunn's method) found differences between miR-133a vs control virus ( $P = 0.002$ ). **C**, representative western blot and fold change in membrane type 1 matrix metalloproteinase (MT1-MMP) abundance in control tissue ( $1.03 \pm 0.059$ ,  $n=11$ ) and TAA tissue transfected with no virus ( $1.38 \pm 0.11$ ;  $n=12$ ), control virus ( $1.24 \pm 0.040$ ;  $n=12$ ), and miR-133a virus ( $0.94 \pm 0.089$ ;  $n=12$ ). \*One-way ANOVA multiple comparisons vs control group (Bonferroni *t* test) found difference between no virus vs control ( $P = 0.005$ ) and control virus vs control ( $P = 0.040$ ). #One-way ANOVA, all pairwise multiple comparison procedure (Tukey test) found difference between no virus vs miR-133a virus ( $P = 0.002$ ) and control virus vs miR-133a virus ( $P = 0.041$ ). In the vertical point plots, the solid line represents the mean, the upper and lower bars represent the standard error of the mean, and the dotted line represents the median.

between the no-virus or control-virus groups with TAA. However, furin suppression by overexpression of miR-133a prevented an increase in active MT1-MMP following TAA induction in mice, and there was no difference when compared with non-TAA control levels ( $0.94 \pm 0.09$ -fold versus  $1.00 \pm 0.07$ -fold;  $n=12$ ;  $P=1$ ) (Figure 7C). Complete uncropped images of the western blots are included in Figure S6.

## DISCUSSION

Results from this set of investigations demonstrate that miR-133a plays a key role in regulating aortic fibroblast phenotype and the development of TAA in an established murine model. Early studies performed by this laboratory identified that TAA progression is accompanied by the emergence of a proteolytically active population of myofibroblasts.<sup>2,16</sup> The current research built on these findings through interruption of this process. We identified alterations in intracellular miR-133a levels have the unique ability to modulate migratory, adhesive, and contractile properties of aortic fibroblasts and

myofibroblasts. Most notably, miR-133a overexpression prevented TAA formation in this murine model. Further examination led to identification of a putative mechanism involved. Specifically, the pro-protein convertase furin was confirmed to be a direct target of miR-133a. Furin is highly expressed in myofibroblasts and regulates the activation of multiple matrix metalloproteinases, consequently contributing to ECM remodeling. The prototypical MT1-MMP is activated by furin and has been demonstrated to play a role in aortic aneurysm formation. Combined, this suggests a common pathway for regulation of adverse proteolytic activity in TAA. Accordingly, this study demonstrated overexpression of miR-133a prevented an elevation in aortic furin levels and subsequent rise in active MT1-MMP. This was sufficient in the attenuation of thoracic aortic aneurysm formation in mice.

In past reports, we identified that the abundance of mature miR-133a was reduced in aortic tissue from patients with TAA.<sup>13,14</sup> In fact, miR-133a levels were found to be inversely proportional to aortic diameter.<sup>14</sup> Interestingly, elevated wall tension applied to the thoracic aorta, as experienced with increased aortic

diameter in TAA, was identified as a mechanism by which miR-133a is reduced in aortic fibroblasts via secretion in exosomes.<sup>19</sup> Consistent with these past reports, the current study was able to demonstrate an inverse linear correlation with aortic diameter and the abundance of miR-133a. As vessel diameter increased, miR-133a was reduced. To this end, it is rational to suggest that reduction in miR-133a may exert an important role in vascular degeneration and dilation associated with TAA development.

To study the initiation and progression of TAA, this laboratory uses a mouse model where aneurysm is induced by placing a sponge soaked in calcium chloride on the periadventitial surface of the descending portion of thoracic aorta. Following exposure, the sponge is removed, and the animals are recovered. Over the time course of aneurysm development, this model consistently demonstrates reproducible progressive dilatation leading to aneurysm formation with evident alterations in the vascular extracellular matrix.<sup>15,16,24–28</sup> Importantly, this TAA model recapitulates the structural hallmarks, changes in cellular content, and alteration in signaling consistent with clinical TAA specimens. Furthermore, these differences correlate with alterations in the transforming growth factor-beta pathway.<sup>28</sup> Altered transforming growth factor-beta signaling, driven in part by both furin and MT1-MMP-mediated release of latent ECM-bound ligand,<sup>22,29</sup> plays a significant role in pathological ECM remodeling and modification of cellular phenotype. This process extensively contributes to development of TAA.<sup>28,30–33</sup> Our current results are consistent with past reports and identified an ~50% increase in aortic diameter at 4 weeks followed by development of a relative plateau in aortic dilation.<sup>2</sup> This suggests 2 distinct phases of aneurysm development. It is during this time that critical changes are occurring, not only in the structural remodeling of the vascular ECM but also in the endogenous cellular composition.<sup>16</sup>

It has been well documented in previous studies that thoracic aortic dilatation is accompanied by smooth muscle cell apoptosis.<sup>5,6</sup> Furthermore, in the thoracic aorta, we do not observe an infiltration of inflammatory cells, as seen in abdominal aortic aneurysm disease.<sup>2</sup> Accordingly, as the aneurysm progresses and the smooth muscle cell content within the thoracic aortic wall decreases, resident fibroblasts become the predominant cell type remaining and likely function to manage the vascular remodeling process. Biochemical identification of fibroblasts is challenging, as they do not contain a single definitive cell marker; however, they do contain proteins that other vascular cells do not. Two such proteins used in studying fibroblasts are vimentin, present in the intermediate filament, and the collagen receptor DDR2. The presence of DDR2 is the more specific of the two. While observed in other cell

types, such as leukocytes, DDR2 is not present in vascular smooth muscle cells or endothelial cells.<sup>2</sup> In addition to changes in cell number, it has been suggested that fibroblasts may undergo a change in phenotype, in response to vascular injury, taking on properties of the myofibroblast.<sup>7</sup> This transdifferentiation event confers specific cell type characteristics. These include increased migratory and contractile properties as well as expression of the smooth muscle cell myosin (Myh11). Thus, the observed elevation in Myh11 copy number in TAA tissue suggested an expansion of myofibroblasts with disease. These changes often result in an altered collagen:elastin ratio because of alterations in deposition and degradation of these critical ECM molecules.

To further examine this unique cellular population, aortic fibroblasts were isolated from non-TAA control and 4-week TAA mice (the time point at which Myh11 expression began to rise) and primary cultures were established.<sup>34,35</sup> The isolated fibroblasts were confirmed to be pure by a highly sensitive method (ddPCR) for detection of mRNA copies of both vimentin and DDR2 and negative for smooth muscle cell-specific desmin and endothelial specific von Willebrand factor. In past reports using this outgrowth technique, a differential gene expression profile was measured by quantitative polymerase chain reaction array to define stable alterations in fibroblasts expanded in culture.<sup>16</sup> The current report built on these past findings by subjecting the fibroblasts to functional phenotypic analyses. The results demonstrated that the TAA fibroblasts had an overall increase in migration and contraction, with a decrease in adhesion when compared with normal control fibroblasts, a profile consistent with myofibroblast behavior. Most importantly, mature miR-133a copy number was found to be significantly reduced in the isolated TAA fibroblasts when compared with controls. The mature miR-133a sequence is transcribed from 2 distinct locations within the genome. Therefore, both primary miR-133a-1 and primary miR-133a-2 levels were quantified. Interestingly, no differences were detected in either primary miR-133a-1 nor primary miR-133a-2, suggesting that regulation of endogenous mature levels occurred after transcription. This result was consistent with a preceding investigation from this laboratory.<sup>19</sup> In this past report, tension reduced intracellular miR-133a by exosome secretion rather than alterations in transcription. Nevertheless, modulation of mature miR-133a levels was sufficient in variation of these functional phenotypes. A remarkable finding from this study was a differential response to miR-133a modulation in the fibroblasts isolated from TAA and control aorta. Specifically, transfection of miR-133a in control fibroblasts did not seem to further reduce migration while having a significant effect in the TAA fibroblasts. Conversely, miR-133a knockdown did not further increase TAA fibroblast migration. This

differential response may suggest the upper and lower ceilings of migratory properties are reached in these fibroblast populations and lack of negative effect on healthy cells gives hope to the possibility of miR-133a as a potential therapeutic.

Most importantly, using this murine model of TAA, we demonstrated that restoration of aortic miR-133a levels in vivo (by lentivirus) attenuated the development of TAA. We successfully demonstrated a >50% increase in diameter in animals that underwent TAA induction, including those that received the nontargeting control virus. Conversely, injection with the miR-133a overexpression virus had a significant attenuation in aneurysm formation. In fact, no difference in aortic diameter measurements were detected when compared with sham-operated controls. Furthermore, this attenuation in TAA formation appeared to persist long term (over the full 16-week time course of the study). Histologically, we were able to recover viral gene expression at 16 weeks. This corresponded with profound differences in medial degeneration across the groups. While aneurysm formation coincided with medial degeneration of elastin, animals that underwent the aneurysm induction that received the miR-133a virus had intact elastic lamellae and an organized collagen network consistent with the representative healthy control aorta. Finally, observation of decreased Myh11 gene expression suggests inhibition of myofibroblast expansion in the animals that received the miR-133a overexpression virus.

As a step toward uncovering a potential mechanism involved with this process, furin was identified as a novel target of miR-133a. Aortic furin levels were observed to be significantly elevated in this murine model of TAA. Following the discovery of furin in 1990, it was regarded as a simple housekeeping protein; however, a crucial role in numerous cellular events has recently triggered investigators to reevaluate the role of furin in disease. Indeed, elevated furin levels have been directly linked to cellular phenotype transformation, tumor progression, metastasis, and vascular remodeling.<sup>36–40</sup> Importantly, furin abundance was elevated in the isolated TAA fibroblasts when compared with healthy controls and protein levels are successfully modulated by overexpression and knockdown of miR-133a alone. Furin is a ubiquitously expressed endoprotease that functions in the proteolytic maturation of a wide portfolio of pro-protein substrates.<sup>41</sup> Furthermore, inhibition has been demonstrated to block >80% of transforming growth factor-beta processing in vitro, suggesting that furin may be a central mediator of ECM remodeling and cellular phenotype transformation in TAA.<sup>22</sup> Phosphorylation and subsequent activation of furin occurs in the endoplasmic reticulum followed by localization to the trans-Golgi network.<sup>42</sup> This includes trafficking between the Golgi, endosomes,

and plasma membrane.<sup>42–44</sup> Nevertheless, the required target sequence of miR-133a, located in the furin 3'UTR, is GACCA. This region of furin transcript, and surrounding sequence, is highly conserved in at least 42 different species, thus indicating inheritance by natural selection. This is exciting and suggests that investigations directed toward miR-133a repression of furin in animal models may aptly translate to humans. Furthermore, this opens up the possibility to reversibly search for other mRNA targets of miR-133a by probing 3'UTR databases.

Another critical pro-protein substrate of furin is MT1-MMP. Furin mediates not only the activation of MT1-MMP but also the levels of functionally active MT1-MMP on the cell surface.<sup>20,45–47</sup> Downstream, MT1-MMP plays a dual role in TAA development through both pericellular proteolysis when on the cell surface and intracellular transforming growth factor-beta signaling when preferentially internalized.<sup>4,23,30,48–50</sup> Therefore, regulation of furin may limit activation of substrates, such as MT1-MMP, thus suppressing pathological ECM remodeling during TAA progression.<sup>36,40,51–56</sup> Accordingly, the proteolytically active, 64-kDa form of MT1-MMP was measured in the aortic tissues. Following aneurysm formation, active MT1-MMP abundance was determined to be elevated in TAA when compared with non-TAA control tissue; however, furin suppression by overexpression of miR-133a prevented an increase in active MT1-MMP and TAA development.

The present study is not without limitations. First, miR-133a was delivered before the formation of TAA. Therefore, effects of miR-133a on an existing aneurysm remain to be determined and will be the focus of future examinations. Second, this investigation focused on the thoracic region of the aorta, while the abdominal portion is also highly susceptible to pathology. Interestingly, there is significant heterogeneity in the structure, function, and response to physiological changes throughout the aorta.<sup>57–59</sup> This highlights the need for ongoing investigations directed at defining the regional differences in the etiology, incidence, and clinical management of aortic disease in the thoracic versus abdominal aorta with respect to levels of miR-133a. Third, in this study we confirmed miR-133a directly modulates furin levels in the thoracic aorta; however, like all microRNAs, miR-133a has multiple targets, some of which assuredly are unidentified. Thus, the effect of furin modulation alone on the development of TAA remain to be determined and will be the focus of future investigations. Finally, lentiviral gene delivery is limited in medical application because of inherent safety concerns. Therefore, we are actively pursuing novel methods for localized delivery and retention of aortic fibroblast miR-133a levels for clinical use.

In summary, thoracic aortic aneurysm disease is often asymptomatic and carries a high level of morbidity



and mortality for which there is currently no effective medical treatment. Dysregulated proteolytic activity is an established mechanism driving TAA formation. This pathological process involves an alteration in resident cellular phenotype known as a fibroblast-to-myofibroblast transition. This weakens the vessel wall, leads to gross dilation, and can progress to rupture in the absence of symptoms. In this report, we identified that miR-133a regulates aortic fibroblast phenotype, and overexpression attenuates proteolytic activation and the development of TAA in a murine model. These unique findings suggest stable alterations in aortic fibroblasts are associated with the development of thoracic aortic aneurysm and regulation by miR-133a may lead to a novel therapeutic strategy.

## ARTICLE INFORMATION

Received October 20, 2020; accepted April 1, 2021.

### Affiliations

Division of Cardiothoracic Surgery, Department of Surgery, University of North Carolina, Chapel Hill, NC (A.W.A., E.N.C., A.R.P., L.B.C., J.K.H., A.D., J.M.T., R.L.V., J.R., A.R., J.E.O., C.M.R., J.S.I.); Division of Cardiothoracic Surgery, Department of Surgery, Medical University of South Carolina, Charleston, SC (J.A.J.); and Research Service, Ralph H. Johnson VA Medical Center, Charleston, SC (J.A.J.).

### Sources of Funding

Research reported in this publication was supported by the National Heart, Lung, and Blood Institute (NHLBI) of the National Institutes of Health: R01HL102121 and R21HL148363 (J.S. Ikonomidis). The content is solely the responsibility of the authors and does not necessarily represent the official views of the National Institutes of Health.

### Disclosures

None.

### Supplementary Material

Table S1

Figures S1–S6

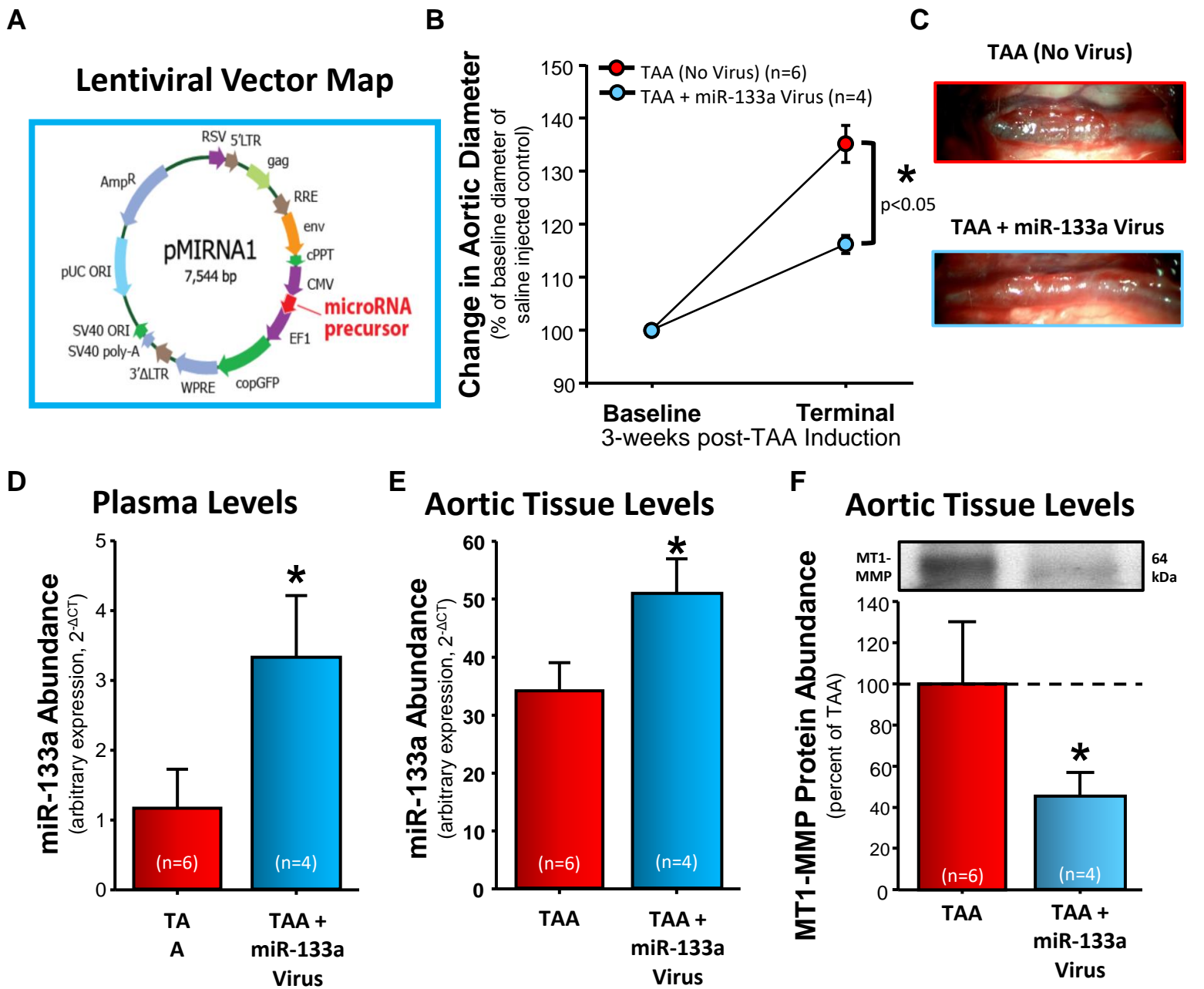
## REFERENCES

- Coady MA, Rizzo JA, Goldstein LJ, Elefteriades JA. Natural history, pathogenesis, and etiology of thoracic aortic aneurysms and dissections. *Cardiol Clin*. 1999;17(615–635):vii. DOI: 10.1016/S0733-8651(05)70105-3.
- Jones JA, Beck C, Barbour JR, Zavadzkas JA, Mukherjee R, Spinale FG, Ikonomidis JS. Alterations in aortic cellular constituents during thoracic aortic aneurysm development: myofibroblast-mediated vascular remodeling. *Am J Pathol*. 2009;175:1746–1756. DOI: 10.2353/ajpath.2009.081141.
- Lindsey ML, Mann DL, Entman ML, Spinale FG. Extracellular matrix remodeling following myocardial injury. *Ann Med*. 2003;35:316–326. DOI: 10.1080/07853890310001285.
- Ikonomidis JS, Nadeau EK, Akerman AW, Stroud RE, Mukherjee R, Jones JA. Regulation of membrane type-1 matrix metalloproteinase activity and intracellular localization in clinical thoracic aortic aneurysms. *J Thorac Cardiovasc Surg*. 2017;153:537–546. DOI: 10.1016/j.jtcvs.2016.10.065.
- Henderson EL, Geng YJ, Sukhova GK, Whittemore AD, Knox J, Libby P. Death of smooth muscle cells and expression of mediators of apoptosis by T lymphocytes in human abdominal aortic aneurysms. *Circulation*. 1999;99:96–104. DOI: 10.1161/01.CIR.99.1.96.
- Sho E, Sho M, Nanjo H, Kawamura K, Masuda H, Dalman RL. Comparison of cell-type-specific vs transmural aortic gene expression in experimental aneurysms. *J Vasc Surg*. 2005;41:844–852. DOI: 10.1016/j.jvs.2005.02.027.
- Zalewski A, Shi Y. Vascular myofibroblasts. Lessons from coronary repair and remodeling. *Arterioscler Thromb Vasc Biol*. 1997;17:417–422. DOI: 10.1161/01.ATV.17.3.417.
- Forte A, Della Corte A, De Feo M, Cerasuolo F, Cipollaro M. Role of myofibroblasts in vascular remodelling: focus on restenosis and aneurysm. *Cardiovasc Res*. 2010;88:395–405. DOI: 10.1093/cvr/cvq224.
- Wei P, Xie Y, Abel PW, Huang Y, Ma Q, Li L, Hao J, Wolff DW, Wei T, Tu Y. Transforming growth factor (TGF)-beta1-induced miR-133a inhibits myofibroblast differentiation and pulmonary fibrosis. *Cell Death Dis*. 2019;10:670.
- Krek A, Grun D, Poy MN, Wolf R, Rosenberg L, Epstein EJ, MacMenamin P, da Piedade I, Gunsalus KC, Stoffel M, et al. Combinatorial microRNA target predictions. *Nat Genet*. 2005;37:495–500. DOI: 10.1038/ng1536.
- Small EM, Frost RJ, Olson EN. MicroRNAs add a new dimension to cardiovascular disease. *Circulation*. 2010;121:1022–1032. DOI: 10.1161/CIRCULATIONAHA.109.889048.
- Desvignes T, Batzel P, Berezikov E, Eilbeck K, Eppig JT, McAndrews MS, Singer A, Postlethwait JH. miRNA nomenclature: a view incorporating genetic origins, biosynthetic pathways, and sequence variants. *Trends Genet*. 2015;31:613–626. DOI: 10.1016/j.tig.2015.09.002.
- Ikonomidis JS, Ivey CR, Wheeler JB, Akerman AW, Rice A, Patel RK, Stroud RE, Shah AA, Hughes CG, Ferrari G, et al. Plasma biomarkers for distinguishing etiologic subtypes of thoracic aortic aneurysm disease. *J Thorac Cardiovasc Surg*. 2013;145:1326–1333. DOI: 10.1016/j.jtcvs.2012.12.027.
- Jones JA, Stroud RE, O'Quinn EC, Black LE, Barth JL, Elefteriades JA, Bavaria JE, Gorman JH III, Gorman RC, Spinale FG, et al. Selective microRNA suppression in human thoracic aneurysms: relationship of miR-29a to aortic size and proteolytic induction. *Circ Cardiovasc Genet*. 2011;4:605–613. DOI: 10.1161/CIRCGENETICS.111.960419.
- Ikonomidis JS, Gibson WC, Gardner J, Sweterlitsch S, Thompson RP, Mukherjee R, Spinale FG. A murine model of thoracic aortic aneurysms. *J Surg Res*. 2003;115:157–163. DOI: 10.1016/S0022-4804(03)00193-8.
- Jones JA, Zavadzkas JA, Chang EI, Sheats N, Koval C, Stroud RE, Spinale FG, Ikonomidis JS. Cellular phenotype transformation occurs during thoracic aortic aneurysm development. *J Thorac Cardiovasc Surg*. 2010;140:653–659. DOI: 10.1016/j.jtcvs.2009.12.033.
- Vernon RB, Gooden MD. An improved method for the collagen gel contraction assay. *In Vitro Cell Dev Biol Anim*. 2002;38:97–101. DOI: 10.1219/01071-2690(2002)038<0097:AIMFTC>2.0.CO;2.
- Alfranca A, Campanero MR, Redondo JM. New methods for disease modeling using lentiviral vectors. *Trends Mol Med*. 2018;24:825–837. DOI: 10.1016/j.molmed.2018.08.001.
- Akerman AW, Blanding WM, Stroud RE, Nadeau EK, Mukherjee R, Ruddy JM, Zile MR, Ikonomidis JS, Jones JA. Elevated wall tension leads to reduced miR-133a in the thoracic aorta by exosome release. *J Am Heart Assoc*. 2019;8:e010332. DOI: 10.1161/JAHA.118.010332.
- Remacle AG, Rozanov DV, Fugere M, Day R, Strongin AY. Furin regulates the intracellular activation and the uptake rate of cell surface-associated MT1-MMP. *Oncogene*. 2006;25:5648–5655. DOI: 10.1038/sj.onc.1209572.
- Dubois CM, Laprise MH, Blanchette F, Gentry LE, Leduc R. Processing of transforming growth factor beta 1 precursor by human furin convertase. *J Biol Chem*. 1995;270:10618–10624.
- Dubois CM, Blanchette F, Laprise MH, Leduc R, Grondin F, Seidah NG. Evidence that furin is an authentic transforming growth factor-beta1-converting enzyme. *Am J Pathol*. 2001;158:305–316.
- Yana I, Weiss SJ. Regulation of membrane type-1 matrix metalloproteinase activation by proprotein convertases. *Mol Biol Cell*. 2000;11:2387–2401. DOI: 10.1091/mbc.11.7.2387.
- Barbour JR, Stroud RE, Lowry AS, Clark LL, Leone AM, Jones JA, Spinale FG, Ikonomidis JS. Temporal disparity in the induction of matrix metalloproteinases and tissue inhibitors of metalloproteinases after thoracic aortic aneurysm formation. *J Thorac Cardiovasc Surg*. 2006;132:788–795. DOI: 10.1016/j.jtcvs.2006.05.052.
- Ikonomidis JS, Barbour JR, Amani Z, Stroud RE, Herron AR, McClister DM Jr, Camens SE, Lindsey ML, Mukherjee R, Spinale FG. Effects of deletion of the matrix metalloproteinase 9 gene on development of murine thoracic aortic aneurysms. *Circulation*. 2005;112:1242–1248.

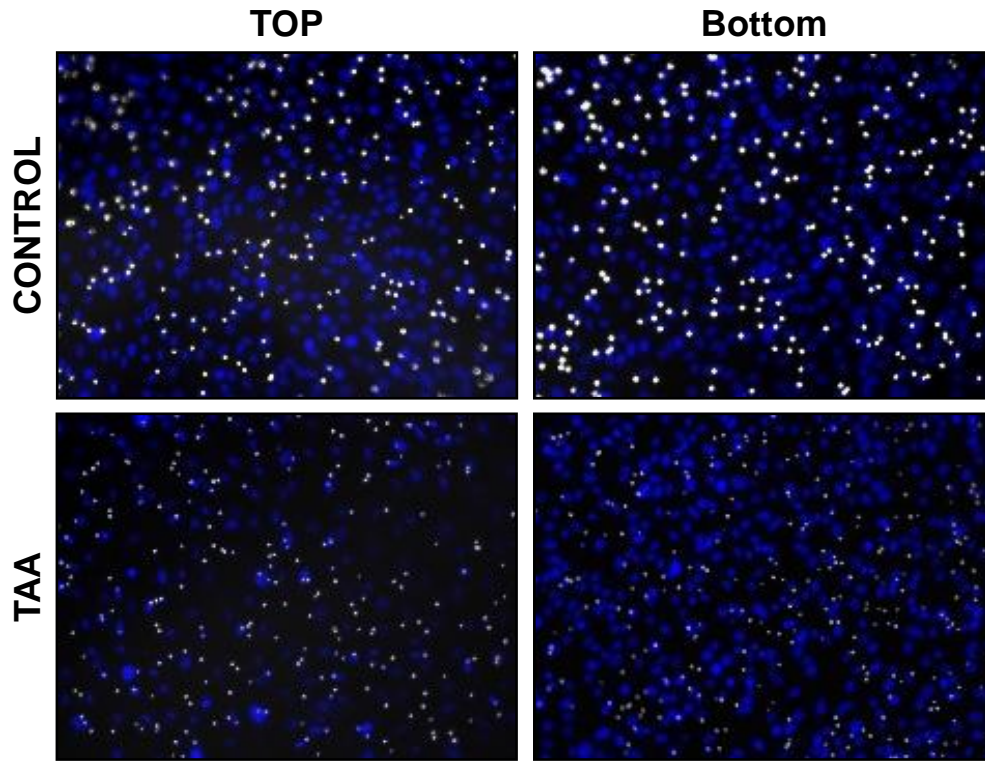
26. Ikonomidis JS, Gibson WC, Butler JE, McClister DM, Sweterlitsch SE, Thompson RP, Mukherjee R, Spinale FG. Effects of deletion of the tissue inhibitor of matrix metalloproteinases-1 gene on the progression of murine thoracic aortic aneurysms. *Circulation*. 2004;110:11268–11273. DOI: 10.1161/01.CIR.0000138384.68947.20.
27. Jones JA, Barbour JR, Lowry AS, Bouges S, Beck C, McClister DM Jr, Mukherjee R, Ikonomidis JS. Spatiotemporal expression and localization of matrix metalloproteinase-9 in a murine model of thoracic aortic aneurysm. *J Vasc Surg*. 2006;44:1314–1321. DOI: 10.1016/j.jvs.2006.07.042.
28. Jones JA, Barbour JR, Stroud RE, Bouges S, Stephens SL, Spinale FG, Ikonomidis JS. Altered transforming growth factor-beta signaling in a murine model of thoracic aortic aneurysm. *J Vasc Res*. 2008;45:457–468. DOI: 10.1159/000127437.
29. Nguyen HL, Kadam P, Helkin A, Cao K, Wu S, Samara GJ, Zhang Q, Zucker S, Cao J. MT1-MMP activation of TGF-beta signaling enables intercellular activation of an epithelial-mesenchymal transition program in cancer. *Curr Cancer Drug Targets*. 2016;16:618–630.
30. Jones JA, Ruddy JM, Bouges S, Zavadzkas JA, Brinsa TA, Stroud RE, Mukherjee R, Spinale FG, Ikonomidis JS. Alterations in membrane type-1 matrix metalloproteinase abundance after the induction of thoracic aortic aneurysm in a murine model. *Am J Physiol Heart Circ Physiol*. 2010;299:H114–H124. DOI: 10.1152/ajpheart.00028.2010.
31. Jones JA, Spinale FG, Ikonomidis JS. Transforming growth factor-beta signaling in thoracic aortic aneurysm development: a paradox in pathogenesis. *J Vasc Res*. 2009;46:119–137.
32. Zile MR, Baicu CF, Stroud RE, Van Laer A, Arroyo J, Mukherjee R, Jones JA, Spinale FG. Pressure overload-dependent membrane type 1-matrix metalloproteinase induction: relationship to LV remodeling and fibrosis. *Am J Physiol Heart Circ Physiol*. 2012;302:H1429–H1437. DOI: 10.1152/ajpheart.00580.2011.
33. Zile MR, Baicu CF, Stroud RE, Van Laer AO, Jones JA, Patel R, Mukherjee R, Spinale FG. Mechanistic relationship between membrane type-1 matrix metalloproteinase and the myocardial response to pressure overload. *Circ Heart Fail*. 2014;7:340–350. DOI: 10.1161/CIRCH.113.000984.
34. Lindsey ML, Goshorn DK, Squires CE, Escobar GP, Hendrick JW, Mingoia JT, Sweterlitsch SE, Spinale FG. Age-dependent changes in myocardial matrix metalloproteinase/tissue inhibitor of metalloproteinase profiles and fibroblast function. *Cardiovasc Res*. 2005;66:410–419. DOI: 10.1016/j.cardiores.2004.11.029.
35. Squires CE, Escobar GP, Payne JF, Leonardi RA, Goshorn DK, Sheats NJ, Mains IM, Mingoia JT, Flack EC, Lindsey ML. Altered fibroblast function following myocardial infarction. *J Mol Cell Cardiol*. 2005;39:699–707. DOI: 10.1016/j.yjmcc.2005.07.008.
36. Thomas G. Furin at the cutting edge: from protein traffic to embryogenesis and disease. *Nat Rev Mol Cell Biol*. 2002;3:753–766. DOI: 10.1038/nrm934.
37. Mercapide J, Lopez De Cicco R, Bassi DE, Castresana JS, Thomas G, Klein-Szanto AJP. Inhibition of furin-mediated processing results in suppression of astrocytoma cell growth and invasiveness. *Clin Cancer Res*. 2002;8:1740–1746.
38. Coppola JM, Bhojani MS, Ross BD, Rehemtulla A. A small-molecule furin inhibitor inhibits cancer cell motility and invasiveness. *Neoplasia*. 2008;10:363–370. DOI: 10.1593/neo.08166.
39. Couture F, Kwiatkowska A, Dory YL, Day R. Therapeutic uses of furin and its inhibitors: a patent review. *Expert Opin Ther Pat*. 2015;25:379–396. DOI: 10.1517/13543776.2014.1000303.
40. Yakala GK, Cabrera-Fuentes HA, Crespo-Avilan GE, Rattanasopa C, Burlacu A, George BL, Anand K, Mayan DC, Corlianò M, Hernández-Reséndiz S, et al. Furin inhibition reduces vascular remodeling and atherosclerotic lesion progression in mice. *Arterioscler Thromb Vasc Biol*. 2019;39:387–401. DOI: 10.1161/ATVBAHA.118.311903.
41. Takahashi S, Nakagawa T, Banno T, Watanabe T, Murakami K, Nakayama K. Localization of furin to the trans-Golgi network and recycling from the cell surface involves Ser and Tyr residues within the cytoplasmic domain. *J Biol Chem*. 1995;270:28397–28401. DOI: 10.1074/jbc.270.47.28397.
42. Molloy SS, Thomas L, VanSlyke JK, Stenberg PE, Thomas G. Intracellular trafficking and activation of the furin proprotein convertase: localization to the TGN and recycling from the cell surface. *EMBO J*. 1994;13:18–33. DOI: 10.1002/j.1460-2075.1994.tb06231.x.
43. Plaimauer B, Mohr G, Wernhart W, Himmelspach M, Dörner F, Schlokot U. "Shed" furin: mapping of the cleavage determinants and identification of its C-terminus. *Biochem J*. 2001;354:689–695. DOI: 10.1042/bj3540689.
44. Mayer G, Boileau G, Bendayan M. Furin interacts with proMT1-MMP and integrin alphaV at specialized domains of renal cell plasma membrane. *J Cell Sci*. 2003;116:1763–1773. DOI: 10.1242/jcs.00394.
45. Boucher E, Mayer G, Londono I, Bendayan M. Expression and localization of MT1-MMP and furin in the glomerular wall of short- and long-term diabetic rats. *Kidney Int*. 2006;69:1570–1577. DOI: 10.1038/sj.ki.5000316.
46. Kang T, Nagase H, Pei D. Activation of membrane-type matrix metalloproteinase 3 zymogen by the proprotein convertase furin in the trans-Golgi network. *Cancer Res*. 2002;62:675–681.
47. Stawowy P, Meyborg H, Stibenz D, Borges Pereira Stawowy N, Roser M, Thanabalasingam U, Veinot JP, Chretien M, Seidah NG, Fleck E, et al. Furin-like proprotein convertases are central regulators of the membrane type matrix metalloproteinase-pro-matrix metalloproteinase-2 proteolytic cascade in atherosclerosis. *Circulation*. 2005;111:2820–2827. DOI: 10.1161/CIRCULATIONAHA.104.502617.
48. Mazzone M, Baldassarre M, Beznoussenko G, Giacchetti G, Cao J, Zucker S, Luini A, Buccione R. Intracellular processing and activation of membrane type 1 matrix metalloproteinase depends on its partitioning into lipid domains. *J Cell Sci*. 2004;117:6275–6287. DOI: 10.1242/jcs.01563.
49. Ikonomidis JS, Jones JA, Barbour JR, Stroud RE, Clark LL, Kaplan BS, Zeeshan A, Bavaria JE, Gorman JH III, Spinale FG, et al. Expression of matrix metalloproteinases and endogenous inhibitors within ascending aortic aneurysms of patients with Marfan syndrome. *Circulation*. 2006;114:1365–1370. DOI: 10.1161/CIRCULATIONAHA.105.000810.
50. Ikonomidis JS, Jones JA, Barbour JR, Stroud RE, Clark LL, Kaplan BS, Zeeshan A, Bavaria JE, Gorman JH III, Spinale FG, et al. Expression of matrix metalloproteinases and endogenous inhibitors within ascending aortic aneurysms of patients with bicuspid or tricuspid aortic valves. *J Thorac Cardiovasc Surg*. 2007;133:1028–1036. DOI: 10.1016/j.jtcvs.2006.10.083.
51. Griffiths G, Simons K. The trans Golgi network: sorting at the exit site of the Golgi complex. *Science*. 1986;234:438–443. DOI: 10.1126/science.2945253.
52. Gu F, Crump CM, Thomas G. Trans-Golgi network sorting. *Cell Mol Life Sci*. 2001;58:1067–1084. DOI: 10.1007/PL00000922.
53. Molloy SS, Anderson ED, Jean F, Thomas G. Bi-cycling the furin pathway: from TGN localization to pathogen activation and embryogenesis. *Trends Cell Biol*. 1999;9:28–35. DOI: 10.1016/S0962-8924(98)01382-8.
54. de Haan CA, Hajjema BJ, Schellen P, Wighers Schreur P, te Lintelo E, Vennema H, Rottier PJ. Cleavage of group 1 coronavirus spike proteins: how furin cleavage is traded off against heparan sulfate binding upon cell culture adaptation. *J Virol*. 2008;82:6078–6083. DOI: 10.1128/JVI.00074-08.
55. Bassi DE, Mahloogi H, Lopez De Cicco R, Klein-Szanto A. Increased furin activity enhances the malignant phenotype of human head and neck cancer cells. *Am J Pathol*. 2003;162:439–447. DOI: 10.1016/S0002-9440(10)63838-2.
56. Jaaks P, D'Alessandro V, Grob N, Buel S, Hajdin K, Schafer BW, Bernasconi M. The proprotein convertase furin contributes to rhabdomyosarcoma malignancy by promoting vascularization, migration and invasion. *PLoS One*. 2016;11:e0161396. DOI: 10.1371/journal.pone.0161396.
57. Ruddy JM, Jones JA, Spinale FG, Ikonomidis JS. Regional heterogeneity within the aorta: relevance to aneurysm disease. *J Thorac Cardiovasc Surg*. 2008;136:1123–1130. DOI: 10.1016/j.jtcvs.2008.06.027.
58. Wolinsky H, Glagov S. Comparison of abdominal and thoracic aortic medial structure in mammals. Deviation of man from the usual pattern. *Circ Res*. 1969;25:677–686. DOI: 10.1161/01.RES.25.6.677.
59. Wolinsky H. Comparison of medial growth of human thoracic and abdominal aortas. *Circ Res*. 1970;27:531–538. DOI: 10.1161/01.RES.27.4.531.

# **Supplemental Material**

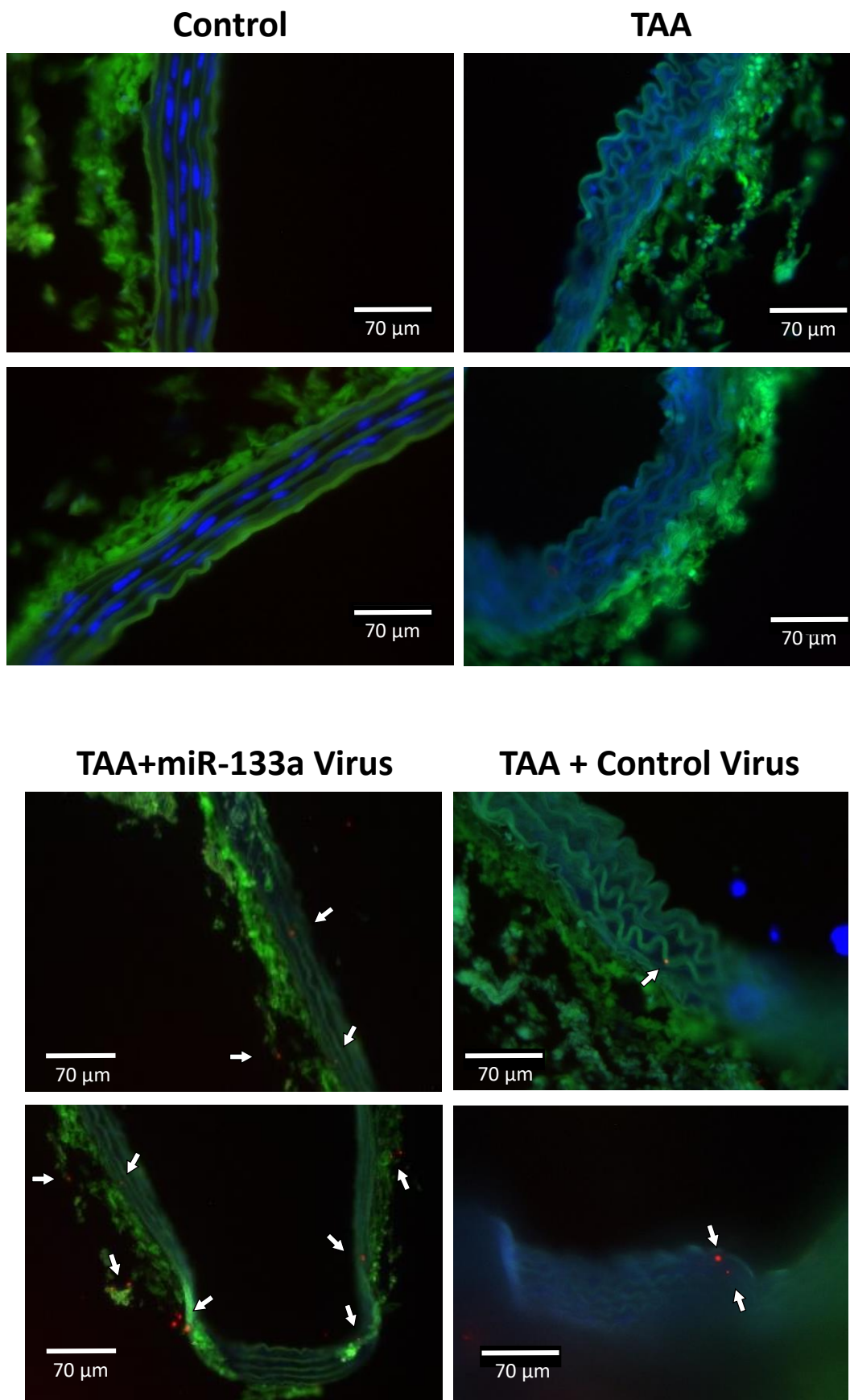
**Table S1. Statistics and data summary (see Excel file).** Data from each figure is displayed as the group sample size (n), mean (m), median, standard deviation (Stdev), standard error of the mean (SEM), mean difference (m1-m2), Effect Size (ES), ES Model used, and p value with corresponding test used. For each ES value an effect level was assigned using the following scheme: <0.1: Trivial; 0.1-0.3: Small; 0.3-0.5: Medium; >0.5: Large.



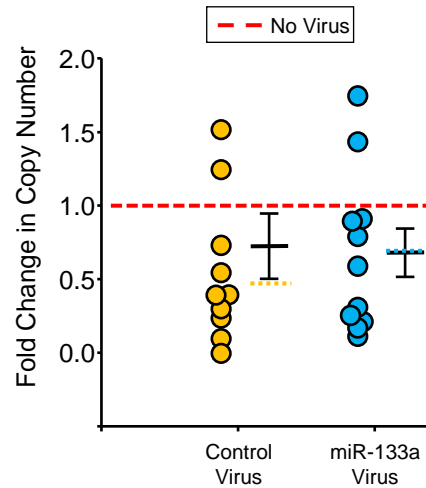
**Figure S1.** Results from pilot studies demonstrating feasibility of miR-133a overexpression on TAA development in mice. **(A)** Lentivirus vector map provided by System Biosciences. This is the vector backbone utilized in the current study for the purposes of overexpressing either the miR-133a precursor (miR-133a Virus), or scrambled sequence control (Control Virus). **(B)** Aortic diameter measurements 3 weeks following TAA induction in mice with or without a single tail-vein injection of the miR-133a virus. **(C)** Gross anatomical images of the descending thoracic aorta 3 weeks following the induction procedure in mice with or without a single tail-vein injection of the miR-133a virus. Significant dilation was observed in mice without miR-133a over expression. **(D)** Three weeks following TAA induction plasma was harvested from mice with or without a single tail-vein injection of the miR-133a virus. RT-PCR was performed on isolated total RNA comparing circulating levels of miR-133a. An elevation of miR-133a levels was detected in mice with received the miR-133a overexpression virus, suggesting successful viral delivery. **(E)** Three weeks following TAA induction the descending thoracic aorta was harvested from mice with or without a single tail-vein injection of the miR-133a virus. RT-PCR was performed on isolated total RNA comparing tissue levels of miR-133a. An elevation of miR-133a levels was detected in mice with received the miR-133a overexpression virus, suggesting successful up-regulation of miR-133a in the thoracic aorta. **(F)** Three weeks following TAA induction, the descending thoracic aorta was harvested from mice with or without a single tail-vein injection of the miR-133a virus. Total protein was subjected to western blotting for a downstream effector of miR-133a, MT1-MMP. A reduction in the active form of MT1-MMP suggested a functional effect of systemic miR-133a over expression. In the vertical bar graphs, the bar represents the mean and the error bar represents the upper standard error of the mean. Student's t-test found differences between TAA and TAA+miR-133a virus in B, and D-F. \* ( $P < 0.05$ )



**Figure S2.** Representative images of the transwell migration assay to accompany the data presented in Figure 3A. Nuclei were stained with DAPI (blue) and images were acquired at 10X in five separate locations on the top and bottom of the 8.0  $\mu\text{m}$  porous fluroblock membranes (corning). Transmitted light images were overlaid with fluorescent images to prevent accidental counting of the pours (which appear as white dots) as nuclei (blue fluorescence). Average cell count for each side was calculated and the percent migration was determined by dividing the average of the bottom membrane count by sum of cell count on top and bottom.

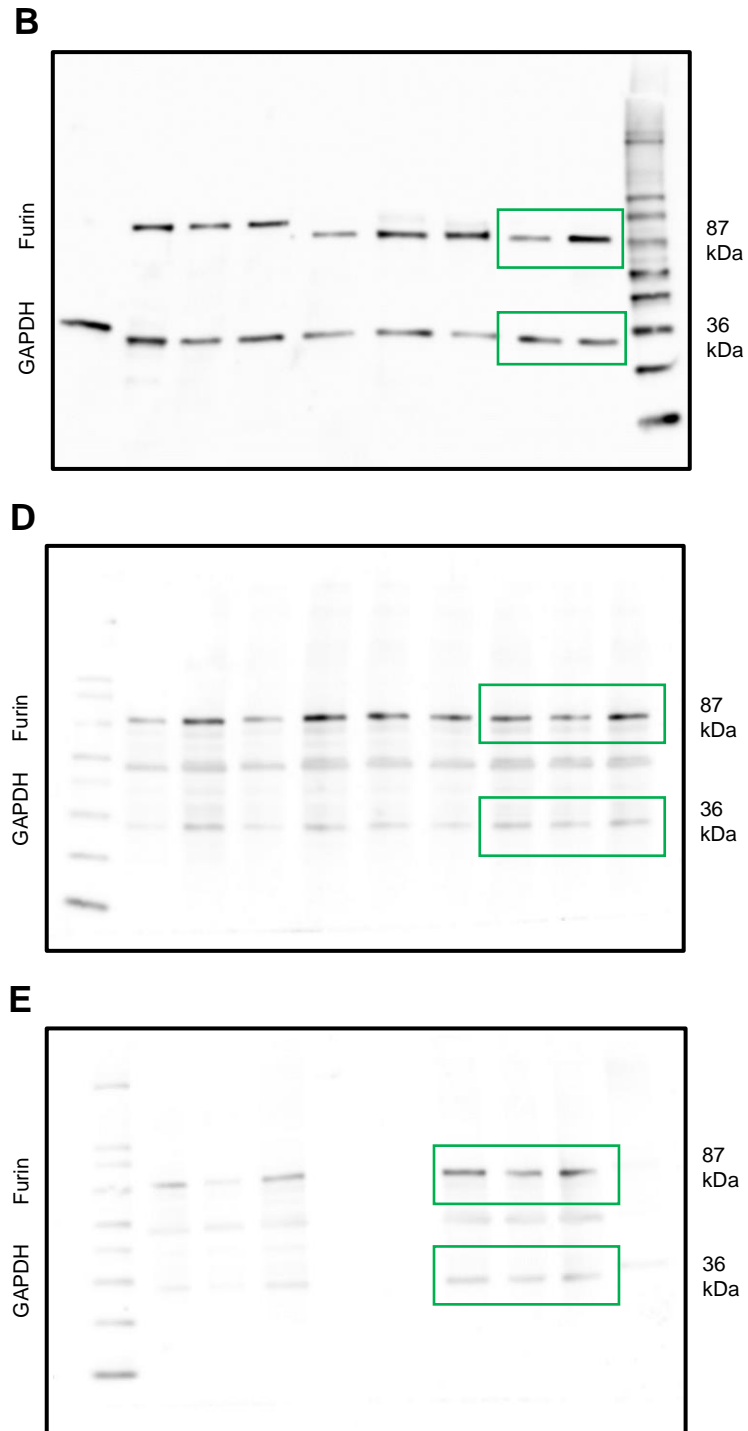


**Figure S3.** Additional fluorescent images of the murine aorta to accompany figure 5C. Immunofluorescence images of non-TAA control (imaged at 20X) and non-transfected (No Virus) (imaged at 20X) and transfected mice with the control virus (imaged at 20X), and miR-133a virus (imaged at 10X) aortic sections 16 weeks following the TAA induction procedure; all scale bars are 70 μm. In the immunofluorescent images, elastin is seen as green auto fluorescence, nuclei are stained blue with DAPI and red is a primary antibody to the green fluorescent protein conjugated with a secondary antibody labeled with a red Alexaflour. White arrows indicate transduced cells labeled with the red Alexaflour. Size bars are included in each image as a white bar.

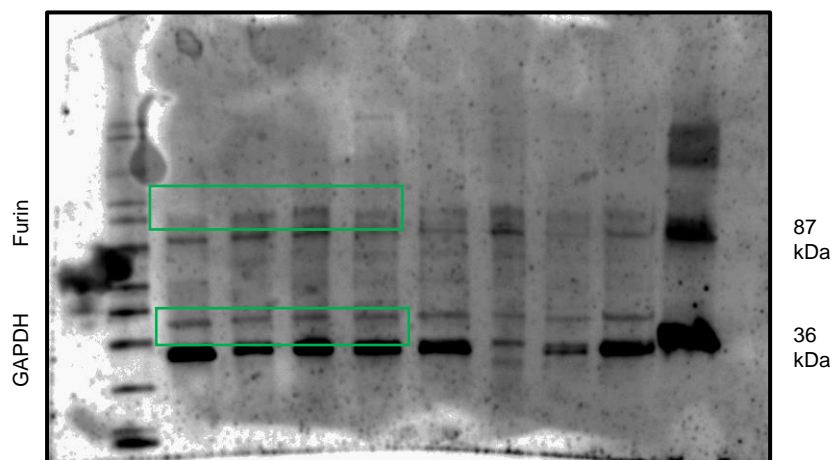
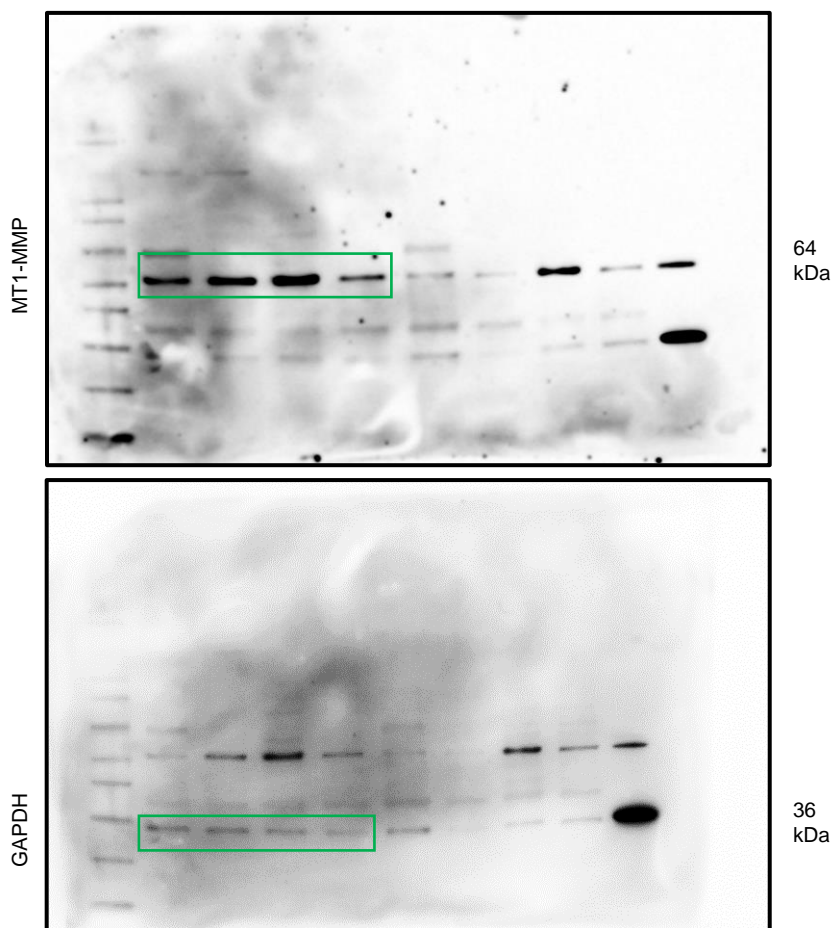


**Figure S4.** Fold change in aortic tissue  $\alpha$ SMA copy number per DDR2 copy following TAA induction in mice transfected with either the control virus ( $0.80 \pm 0.23$  fold) or the miR-133a over expression virus ( $0.68 \pm 0.16$  fold) compared to non-transfected mice with TAA (red dashed line) ( $n = 11$ ). \* Student's t-test and Welch's t-test found no difference between miR-133a virus versus control virus ( $P = 0.86$ ).





**Figure S5.** Full blot images from figure 6. Included are the complete, uncropped images of the nitrocellulose membranes accompanying the data presented in figure 6. The green box indicates the areas that were quantified by densitometry.

**B****C**

**Figure S6.** Full blot images from figure 7. Included are the complete, uncropped images of the nitrocellulose membranes accompanying the data presented in figure 7. The green box indicates the areas that were quantified by densitometry.